# CYCLIC SEDIMENTATION IN THE MISSISSIPPIAN PRIDE SHALE: QUANTITATIVE PALEOENVIRONMENTAL ANALYSIS OF TIDAL RHYTHMITES USING X-RAY FLOURESCENCE SCANNING AND ADVANCED SPECTRAL METHODS

Kristin Heather Larkins

A thesis submitted to the faculty of the University of North Carolina at Chapel Hill in partial fulfillment of the requirements for the degree of Master of Sciences in the Department of Geological Sciences

Chapel Hill
2009

Approved by:

Stephen R. Meyers

Louis R Bartek

Kevin Stewart

## ABSTRACT

Kristin Larkins: Cyclic Sedimentation in the Mississippian Pride Shale:
Quantitative Paleoenvironmental Analysis of Tidal Rhythmites
Using X-Ray Fluorescence Scanning and Advanced Spectral Methods
(Under the direction of Dr. Stephen Meyers and Dr. Lou Bartek)

Tidal rhythmites offer an opportunity to constrain the orbital dynamics of the Earth-Sun-Moon system, and potentially provide high-resolution paleoclimate archives. In this study, we develop a new methodology for the investigation of ancient tidal rhythmites, using high-resolution X-ray fluorescence (XRF) scanning and advanced spectral methods. Importantly, the XRF-scanning technique provides the opportunity to evaluate multiple paleoenvironmental signals (e.g., detrital, biogenic, and authigenic contributions) preserved within these deposits, and thus allows a more complete analysis of their mechanism of formation. Assessment of the individual paleoenvironmental proxy records using advanced spectral methods permits evaluation of their linkage to specific tidal and climatic forcing agents. As a case study, we investigate the Mississippian Pride Shale of West Virginia, an unusually thick tidal rhythmite deposit (~60 m), representing hundreds to thousands of years of sedimentation. Our analyses suggest robust detrital, biogenic, and redox proxies, with variable sensitivity to the individual forcing mechanisms.

## ACKNOWLEDGEMENTS

I would like to thank the West Virginia Geological Survey and the University of North Carolina Martin Fund for support in this research project. I would also like to thank my research advisors for their support and knowledge. Most of all, I would like to thank my parents and husband for their support while undertaking this project.

**TABLE OF CONTENTS**

## LIST OF TABLES

Table

## LIST OF FIGURES

Figure

# CHAPTER 1

# INTRODUCTION AND BACKGROUND

## 1.1 Introduction to the Problem

Ancient tidal rhythmites have been widely investigated to constrain past orbital dynamics (e.g., changes in the length of day and Earth's precession constant; Sonett et al., 1996; Kvale et al., 1999; Berger et al., 1989), and to reconstruct paleoenvironment (e.g., Miller, 1998). A wide range of methodologies have been employed for such purposes, ranging from sedimentologic and stratigraphic (Hovikoski et al., 2005) to numerical ocean models (Wells et al., 2007). However, few if any studies have taken a multi-proxy geochemical approach to the analysis of ancient tidal rhythmites. Importantly, quantification of detrital, biogenic, and authigenic signals preserved in tidal rhythmite geochemistry provide the opportunity for a far more complete understanding of their mechanism of formation, including the extraction of distinct tidal and climatic (e.g., monsoonal) forcings. The advent of new X-Ray Fluorescence (XRF) scanning methodologies (Richter et al., 2006) now provides the opportunity to attain the high-resolution geochemical records required for such purposes.

In this study, we develop a new approach to the analysis of tidal rhythmites, which utilizes the high-resolution XRF-scanning technique, and advanced spectral methods (multi-taper method time-frequency analysis, coherency analysis; Thomson, 1982). The

methodology is specifically designed to deconvolve multiple paleoenvironmental signals preserved in tidal rhythmites, and to evaluate their linkage to specific forcing mechanisms. As a test case we investigate the Mississippian Pride Shale of southeastern West Virgina, which represents an exceptionally long record of tidal deposition (likely hundreds to thousands of years), potentially the longest of the entire Phanerozoic (Miller, 1998). Two primary hypotheses pertaining to the Pride Shale that we will test include:

Hypothesis 1: The geochemistry of the Pride Shale rhythmites preserves multiple paleoenvironmental signals (e.g., detritial, biogenic, and authigenic contributions)

Hypothesis 2: The quality of the Pride Shale rhythmite record (completeness, etc.) varies from distal to proximal prodeltaic settings.

The results of this study demonstrate the power of the new methodology, and have important implications for the paleoenvironmental mechanisms controlling Pride Shale rhythmite formation. The analysis of both distal and proximal depositional environments allows us to compare and contrast formation mechanisms in distinct basin settings, and enables us to locate the ideal sampling area to extract tidal frequencies using spectral analysis. This new technique can be applied to other ancient tidal rhythmites to constrain tidal and paleoclimatic forcings, and to evaluate changes in Earth's celestial mechanics.

## 1.2 Background: Tidal Rhythmites and Their Quantitative Analysis

Tidal rhythmites are sedimentary packages of sandstone, siltstone, and/or mudstone that are of tidal origin, and contain some rhythmicity in either grain size or thickness of beds

(Williams, 1991; Kvale, 2003; Mazumder and Arima, 2004). The formation of tidal rhythmites is dependent on the Earth-Moon-Sun system, and thus tidalites are potentially an excellent tool for reconstructing the evolution of this system through time (Kvale et al., 1999; Mazumder and Arima, 2004). For example, analysis of rhythmites from the Proterozoic Big Cottonwood Formation in Utah derived a value of 31.1 solar days per month, compared to the modern day value of 29.5 solar days per month (Sonnett et al., 1996). Considering several other tidal rhythmites units, Sonnett et al. (1996) determined that the length of the solar month has decreased over time at a constant rate due to tidal friction. Similarly, Williams (1997) compiled the results of several tidal rhythmite studies to calculate Precambrian values of tidal, rotational and orbital parameters, such as the length of the day and rate of lunar retreat. Analysis of the rhythmites indicates that the solar year length has decreased over time, from 465 ± 16 days per year during the Proterozoic to the current 365.24 days per year.

Lamination thickness is frequently investigated in tidal rhythmites studies because it is dependent upon the tidal range and current strength (Mazumder and Arima, 2004). High tides are recognized by thicker laminae, while lower tides are recorded as thin laminae (Mazumder and Arima, 2004), producing a thick-thin bundle ("cycle") of sediment. Today, a semidiurnal system will record 28 of these thick-thin bundles during a neap-spring cycle, while a dominantly diurnal system will record 14 cycles during neap-spring cycle (Kvale, 2006; Mazumder and Arima, 2004). Thus, a timeseries plot of cycle number versus cycle thickness is typically used to yield insight into the paleotidal system present (Mazumder, 2004).

A common approach employed in tidal rhythmite research is to analyze these cycle thickness timeseries via spectral methods to quantify the dominant periods. The Fast Fourier transform and maximum entropy methods have both been used to resolve the tidal frequencies (Archer et al., 1991; Miller, 1998; Mazumder and Arima, 2004). However, tidal rhythmites may also contain hiatuses or bioturbated layers, as well as evidence of storms or other phenomena, which can affect the analysis of temporal frequencies in the data. If these sedimentary distortions are minimal, or can be quantified and resolved using advanced spectral methods (e.g., Evolutive Harmonic Analysis; Meyers et al., 2001), tidalites can serve as an excellent tool for revealing ancient orbital dynamics. In this study, we will apply advanced spectral techniques and XRF-scanning to deconvolve multiple paleoenvironmental signals preserved in the geochemistry of ancient tidal rhythmites, and we will also use the spectral methods to constrain sedimentary distortions of the periodic signals.

## 1.3 Background: The Pride Shale

The Mississippian Pride Shale outcrops in southeastern West Virginia along a belt that trends southeast-northwest from Tennessee to Pennsylvania along the Appalachians (Figure 1) as part of the Bluestone Formation (Reger, 1926). Sediment was sourced from tectonic highlands in the eastern Appalachian basin (Englund and Thomas, 1990). This is illustrated by the NW-SE trend of the Pride Shale deposition as part of a clastic wedge, where accommodation was created by subsidence due to thrust loading in the central basin (Ettensohn, 1994; Rice and Schwietering, 1988).

The Pride Shale was first described by Reger (1926), and overlies the Princeton Sandstone (Figure 2). It comprises a ~60 meter thick unit of shales, siltstones, and fine-

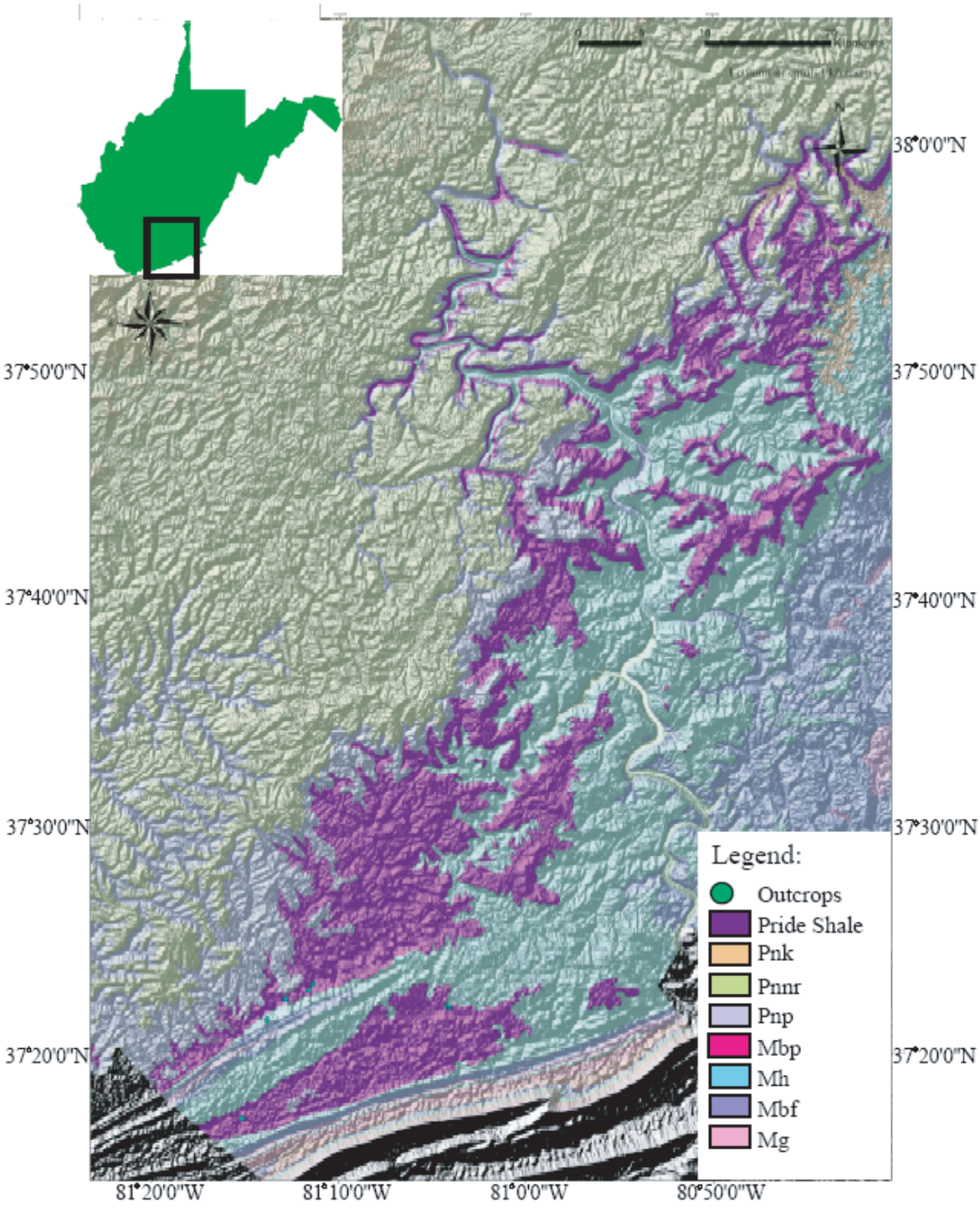


Figure 1. Location map showing the extent of the Pride Shale along a southwestern tend in the Appalachian mountains. Pnk = Kanawha Fm, Pnnr = New River Fm, Pnp = Pocahontas Fm, Mbp = Bluestone and Princeton Fm, Mh = Hinton Fm, Mbf = Bluefield Fm, Mg = Greenbriar Grp. Map data from the www.usgs.gov.

Figure 2. Photograph of the Pride Shale at Camp Creek, WV along Interstate-77, displaying the lithologic rhythmicity that is characteristic of this unit. A Jacob's staff (1 meter) is shown for scale.

grained sandstones that display a striking visual cyclicity (Miller, 1998; Figure 2). The base of the Pride Shale is recognized by a black, fissile shale, that records a high gamma ray signature (Figure 3), which is interpreted to be a condensed section that formed during a maximum flooding event (Miller, 1998). This condensed section is observed throughout the extent of the Pride Shale, which coarsens upward into the rhythmically bedded shale, siltstone, and fine-grained sandstone. At its uppermost extent, the Pride Shale grades into the Glady Fork Member (Figure 4), a wavy-bedded, fine-grained sandstone unit that also exhibits some visual cyclicity.

Large, concave-upward discontinuities are present within the most laterally continuous portion of the Pride Shale along Interstate 77 at Camp Creek, West Virginia. These discontinuities have been interpreted alternatively as slump-blocks (Cooper, 1961) and channel scours (Englund, 1989). In addition, Miller and Eriksson (1997) have proposed an infilled slump scar origin for the discontinuities, which they suggest is created by subaqueous gravity sliding of coherent blocks of sediment, followed by infill associated with prodeltaic sedimentation.

Plant fossils (*Stigmaria stellata*) and bivalves (*Sanguinolites, Modiolus sp.*) are localized in the Pride Shale, while shrimp-like arthropod imprints are found upsection (Miller, 1998). Bioturbation is not a prominent feature; however evidence for bioturbation is more common in the sandier facies. Sparse fossil and plant material indicate a paleoenvironment where large salinity fluctuations or anoxic conditions excluded benthic fauna (Miller, 1998). Furthermore, paleosols in the underlying Hinton Formation and Bluestone Formation (Cecil and Englund, 1989), as well as Mississippian paleo-vertisols in Tennessee, suggest a semi-arid climate during this time (Caudill et al., 1996).

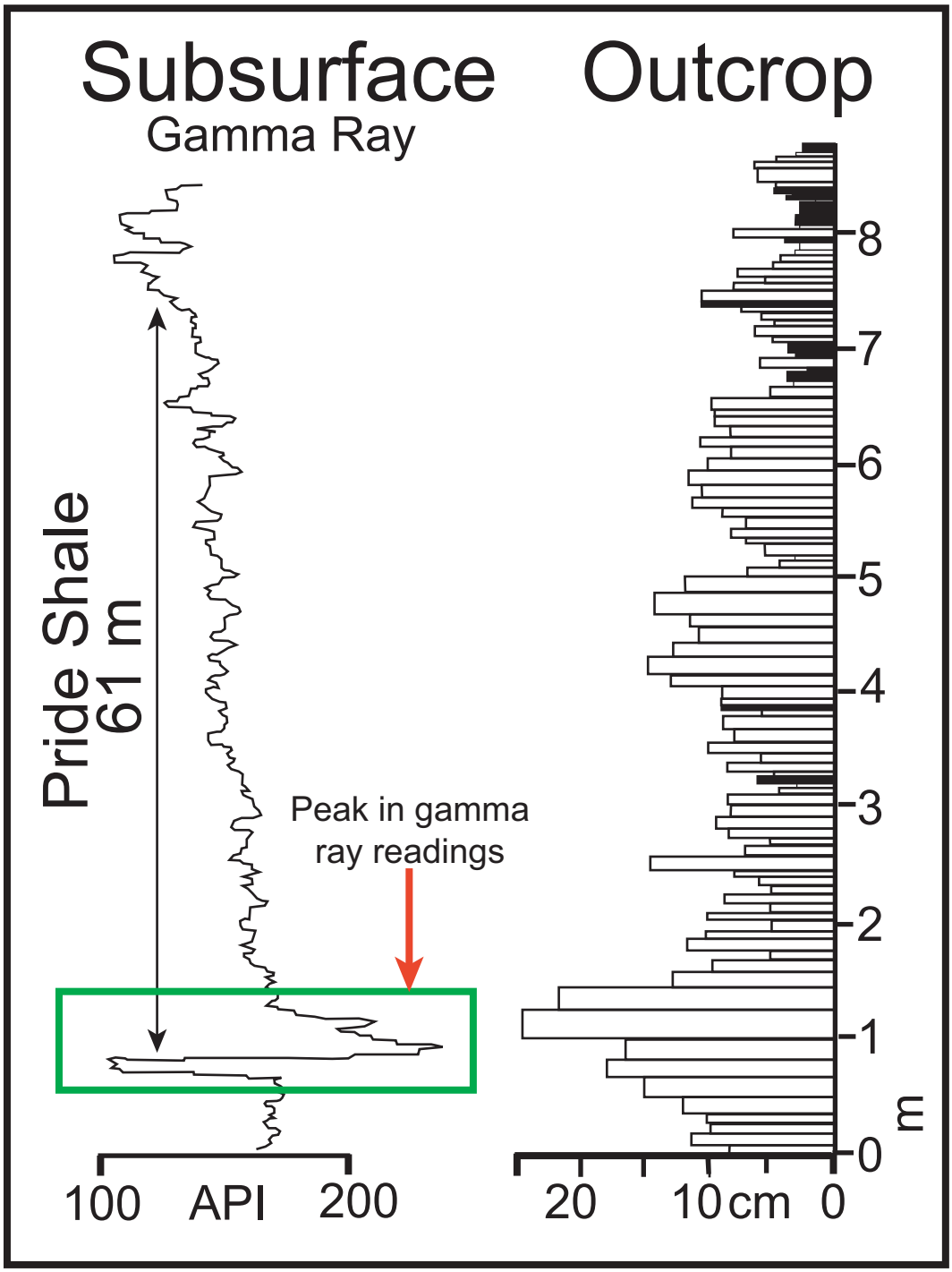


Figure 3. Gamma ray log of the Pride Shale, showing the high gamma ray signature that defines the base of the Pride Shale in the subsurface. This high gamma ray signature is attributed to a condensed section created by a transgressive shoreline. The right side of the diagram illustrates the thickening and thinning of meter scaled cycles in outcrop (modified from Miller, 1998).

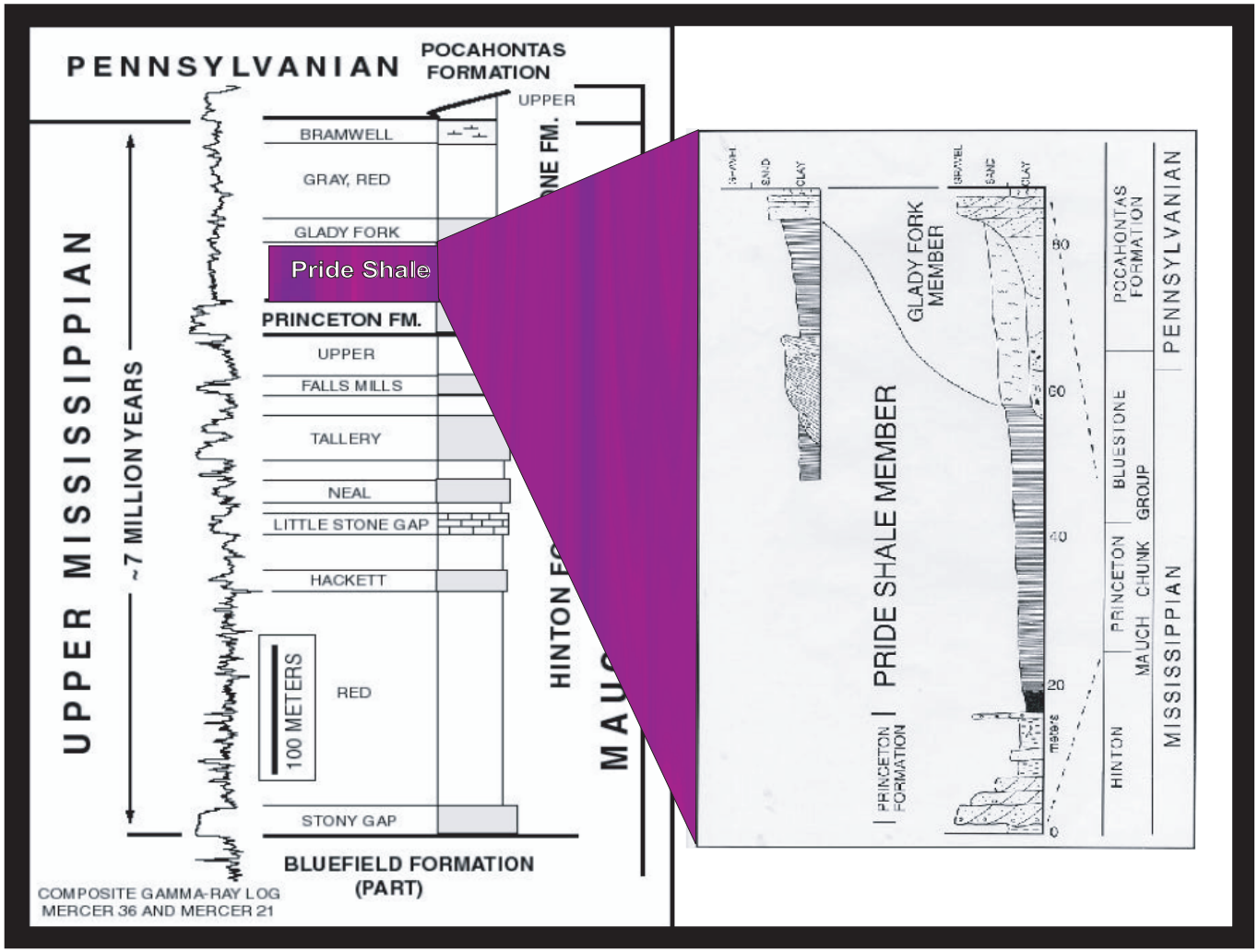


Figure 4. Stratigraphic column of the Pride Shale unit, with the inset illustrating the gradation from shaly strata into the more sandy Glady Fork Member (modified from Miller, 1998).

## 1.4 Background: Source of the Pride Shale Rhythms

The source of the rhythms observed in the Pride Shale has been a subject of great debate. Relevant to this issue, previous researchers have suggested a range of depositional environments for the Pride Shale laminated sequence, including a low-energy tidal depositional environment (Cecil and Englund, 1989), a shallow-marine lagoonal or estuarine environment, (Miller, 1974; Englund, 1989), and a deltaic environment (Englund and Thomas, 1990). More recently, Miller and Eriksson (1997) have proposed that the Pride Shale formed in a gently sloping, tidally-influenced prodeltaic environment.

Neal (1994) has suggested that the Pride Shale rhythms formed due to seasonal oxygen level changes. Since the condensed section at the base of the Pride Shale signifies maximum inundation of the basin, an annual oxygen level explanation for the millimeter scale couplets may be reasonable for the most distal areas of Pride Shale deposition. However an annual interpretation for these couplets would require an additional explanation of larger scale bundling that is observed in the sediment (Miller and Eriksson, 1997). Alternatively, climate variability associated with sunspot cycles could explain the centimeter-scale couplet packaging within the Pride Shale (see below; Miller and Eriksson, 1997). However, invoking sunspot cycles to explain the centimeter-scale couplets would also require supplementary forcings to explain the decimeter scale and meter scale bundles seen in the Pride Shale sediments (see below; Miller and Eriksson, 1997).

Miller and Eriksson (1997) have described the cyclicity observed in the Pride Shale as a combination of tidal and climatic forcing mechanisms. This interpretation is based on an analysis of couplets and lamination thickness, which were counted in the outcrop setting, as well as thin section sampling of the millimeter scale laminations. The outcrop thickness

observations were analyzed using spectral methods to quantify spatial rhythms in laminae thickness, resulting in the interpretation of a hierarchy of tidal and climatic signals (Figure 5), as well as an 18.6 year lunar nodal cycle. Based on Miller and Eriksson's (1997) estimates, this unit is exceptionally long, representing hundreds to thousands of years of rhythmite deposition.

A prodeltiac environment was proposed by Miller and Eriksson (1997) to account for the preservation of the long tidal record. A prodeltaic environment is a relatively stable area where sediments are deposited from suspension, creating laminations in some cases (Reading and Collinson, 1996). Miller and Eriksson (1997) and Miller (1998) interpret the Pride Shale as a prodelta based on the lateral extensiveness of the unit, sedimentological features, and the stratigraphic relationships bounding the unit.

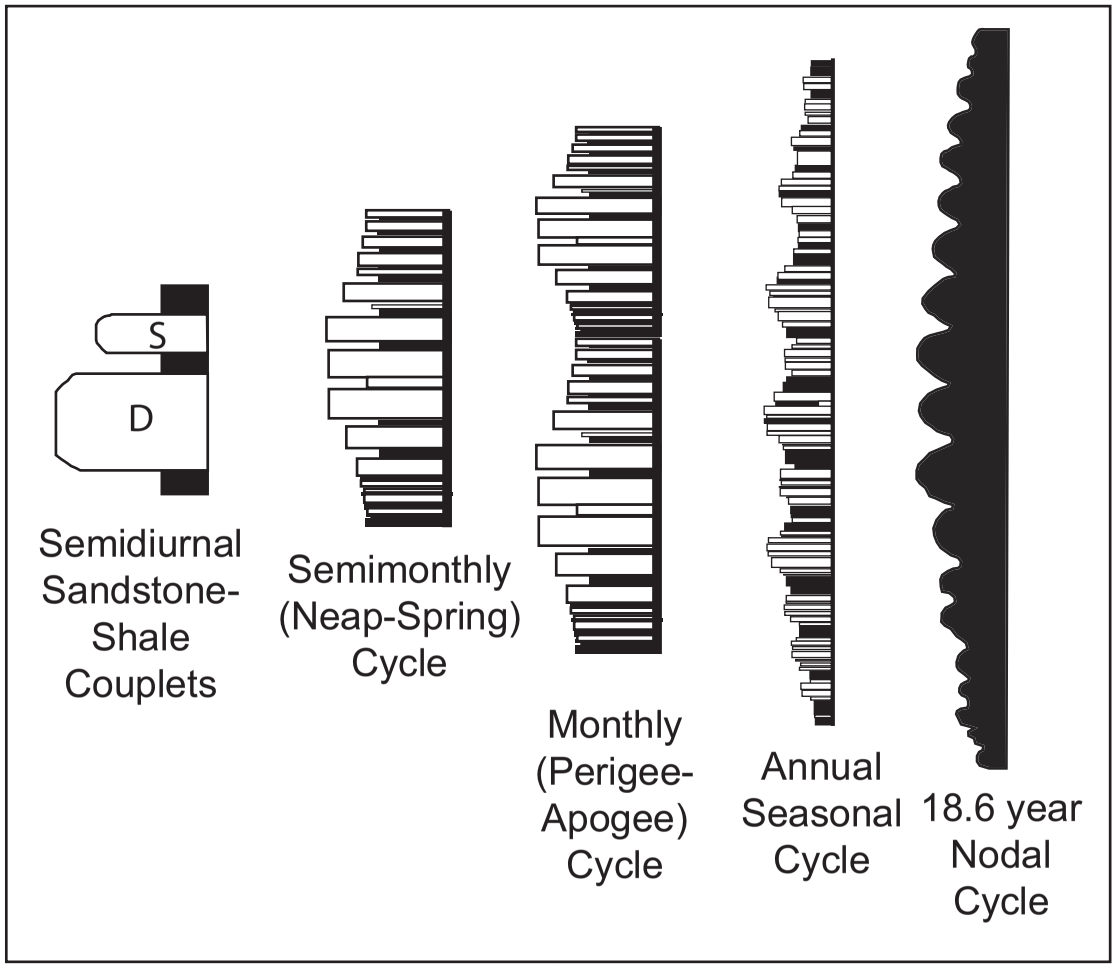


Figure 5. Miller and Eriksson's (1997) previous interpretations of the rhythmicity in the Pride Shale included cycles from daily to multi-year cycles. These interpretations were based on visual observations in the field, as well as from photomicrographs of the Pride Shale. Figure modified from Miller and Eriksson (1997).

# CHAPTER 2

# A NEW METHODOLOGY FOR QUANTITATIVE PALEOENVIRONMENTAL ANALYSIS OF TIDAL RHYTHMITES: XRF-SCANNING AND ADVANCED SPECTRAL METHODS

## 2.1 Introduction

In this study, a combination of XRF-scanning and advanced spectral methods are applied to provide insight into tidal rhythmite formation and the basin dynamics present during their deposition. The XRF-scanning methodology provides high-resolution profiles of a wide range of geochemical components. These XRF-geochemical data potentially provide valuable information about detrital and biogenic contributions to the depositional system, as well as redox state (authigenic contributions). Detailed quantitative analysis of the geochemical proxy data will be conducted using advanced spectral methods to determine the periodicities recorded in the rhythmites, and will be used to link the different environmental parameters to specific forcing mechanisms (tidal versus climatic). Evaluation of the tidal rhythmites is supplemented by optical thin section and SEM analyses, which are used to groundtruth our interpretations of the proxy signals in the record. This new interdisciplinary approach to tidal rhythmite analysis will assist in understanding the mechanism of tidalite formation and orbital dynamics.

### 2.2.1 Multi-proxy Geochemical Analysis via XRF-scanning

A wide array of information about tidal environments is preserved within the chemistry of tidal rhythmites. Due to their coastal marine nature, tidal rhythmites can potentially preserve material derived from marine and terrigenous sources, including detritial, biogenic, and authigenic contributions.. Detritial input is the sedimentation due to land-derived sources, such as riverine input due to precipitation runoff. Biogenic input refers to material sourced from biologic influences, such as marine algal blooms or calcareous tests, as well as land-derived organic matter. Authigenic input is sedimentation created in situ, for example, iron sulfides produced within marine sediment associated with bacterial sulfate reduction (Berner, 1970). Although these different components may be preserved in tidal rhythmites, this type of data has been a relatively untapped resource in ancient tidalite research due to a previous lack of instrumentation for routine evaluation of the geochemistry of individual thin laminae.

### 2.2.2 Geochemical Proxies for Detrital, Biogenic, and Authigenic Sediment Sources

Titanium and aluminum are particularly useful detrital proxies. These elements can be derived from riverine detrital input into a basin, as well as eolian detrital input from arid regions (Sageman and Lyons, 2004; Lantzy and Mackenzie, 1979; Yarincik et al., 2000b). In continental shelf and slope environments, aluminum has been previously used as a conservative proxy for clay minerals derived from crustal weathering. In contrast, titanium is commonly associated with Ti-rich silt to sand sized grains (e.g., rutile) (Bertrand et al., 1996). Thus, changes in the character of the detrital input to the basin can be detected using the elemental ratio of aluminum to titanium (Sageman and Lyons, 2004). As a detrital proxy,

total titanium content has also been previously used to determine changes in runoff from land sources into oceanic basins (Haug et al., 2001).

A second source of sediment to a depositional basin is the biogenic input due to primary production. Biogenic silica and calcium have been effectively used to quantify the biogenic contribution to the sediment (Sageman and Lyons, 2004). However, analysis of bulk silicon and calcium variability as a proxy for biogenic activity is complicated by the fact that silicon and calcium can also be derived from detrital sources. To resolve this problem, robust detrital components such as titanium can be used in combination with silicon and calcium to evaluate changes in biogenic input in fine-grained sediments (Si/Ti; Ca/Ti; Davis et al., 1999). Using this approach, it is possible to identify the more productive periods during deposition, which may coincide with particular tidal or climate forcing mechanisms.

The third source of material to sedimentary record is associated with authigenic processes. The formation of authigenic sedimentary components is usually coupled to the remineralization of organic matter (OM). If sufficient labile OM is present, oxygen will be depleted during the metabolism of OM. Once oxygen is depleted a sequence of alternative OM remineralization processes can occur, including Fe-reduction, Mn-reduction, nitrate reduction, sulfate reduction, and methanogenesis (Sageman and Lyons, 2004). Redox sensitive elements such as S, Fe, Mn, V, Cr, Mo, and U can be used to detect associated changes in the redox state of the sediments (Sageman and Lyons, 2004). In many cases this is due to the fact that each microbial regime is characterized by particular redox and pH conditions, which results in the precipitation or scavenging of specific redox sensitive elements.

In this study, we are particularly interested in evaluating changes in the sulfide content of the tidal rhythmites, as a measure of changes in sulfate reduction and pore water oxygen content. Sulfate is commonly abundant in seawater and the uppermost portion of the sediment column, and can facilitate the anaerobic remineralization of organic matter when aerobic respiration has removed oxygen and other energy efficient oxidants from the system (Libes, 2005). Sulfate reduction is an especially important processes in highly restricted or stratified basins (Lyons et al., 2003), due to reduced oxygen replenishment. As sulfate reduction proceeds, the amount of sulfate in the sediment column decreases with depth in the sediment (Figure 6), while the amount of hydrogen sulfides increase (Libes, 2005). The reaction of this dissolved hydrogen sulfide with reactive iron produces iron monosulfides and pyrite (Berner, 1970; Sageman and Lyons, 2004). Thus, the geochemical record of sulfur potentially contains information about the oxygen state in the Pride Shale basin.

### 2.2.3 XRF-scanning methods

Using XRF scanning to evaluate tidal rhythmites, these geochemical signatures can be detected at a very high resolution, providing the necessary continuous record of environmental change that we will investigate in this study. The Avaatech XRF scanner (Figure 7) uses a rhodium anode to produce the x-rays. X-rays bombard the sample causing an electron to be removed from the atom (Jenkins, 1999). When an inner shell electron is removed from the atom, an electron from an outer shell falls in to replace the missing electron, resulting in an energy change. This energy change is associated with the emission of a photon of a particular frequency, which is measure by the x-ray detector (Figure 8) (Jenkins, 1999). Each element contains a signature frequency fingerprint, which is then used

(A) Sulfate Reduction

$$SO_4^{2-} + 2(CH_2O) = H_2S + 2HCO_3^-$$

(B)

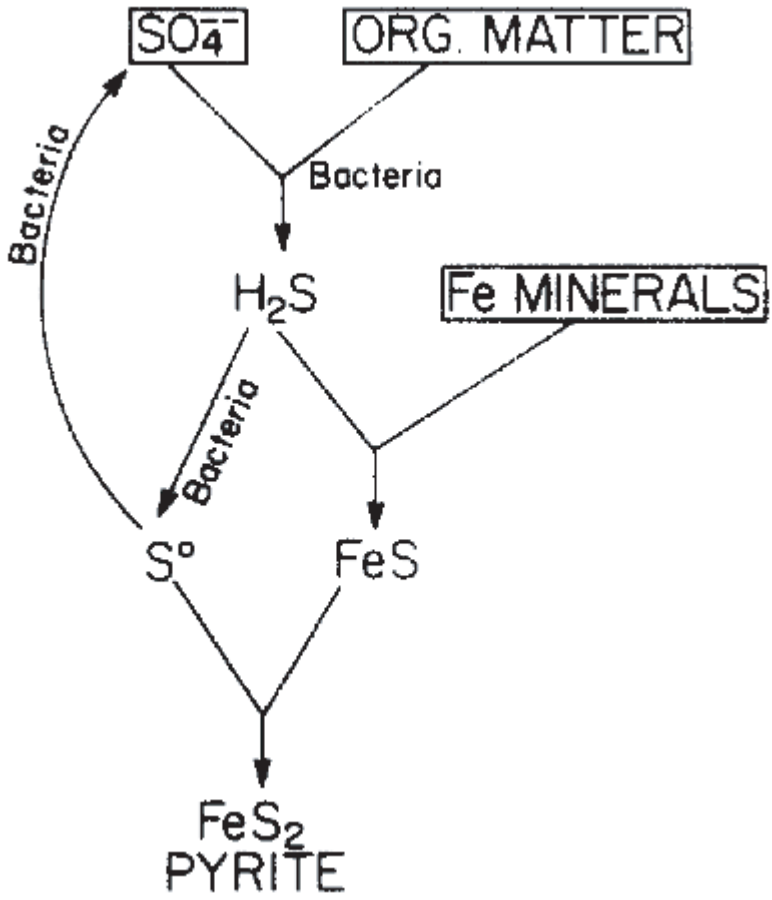


Figure 6. (A) The sulfate present in seawater and pore water is reduced to hydrogen sulfide as organic matter is decomposed via sulfate reduction. (B) This hydrogen sulfide reacts with iron minerals to produce iron monosulfide, and after further reaction with elemental sulfur, pyrite is formed. Figure 6B from Berner (1984).


Figure 7. Photograph of the Avaatech XRF-core scanner at the University of North Carolina.

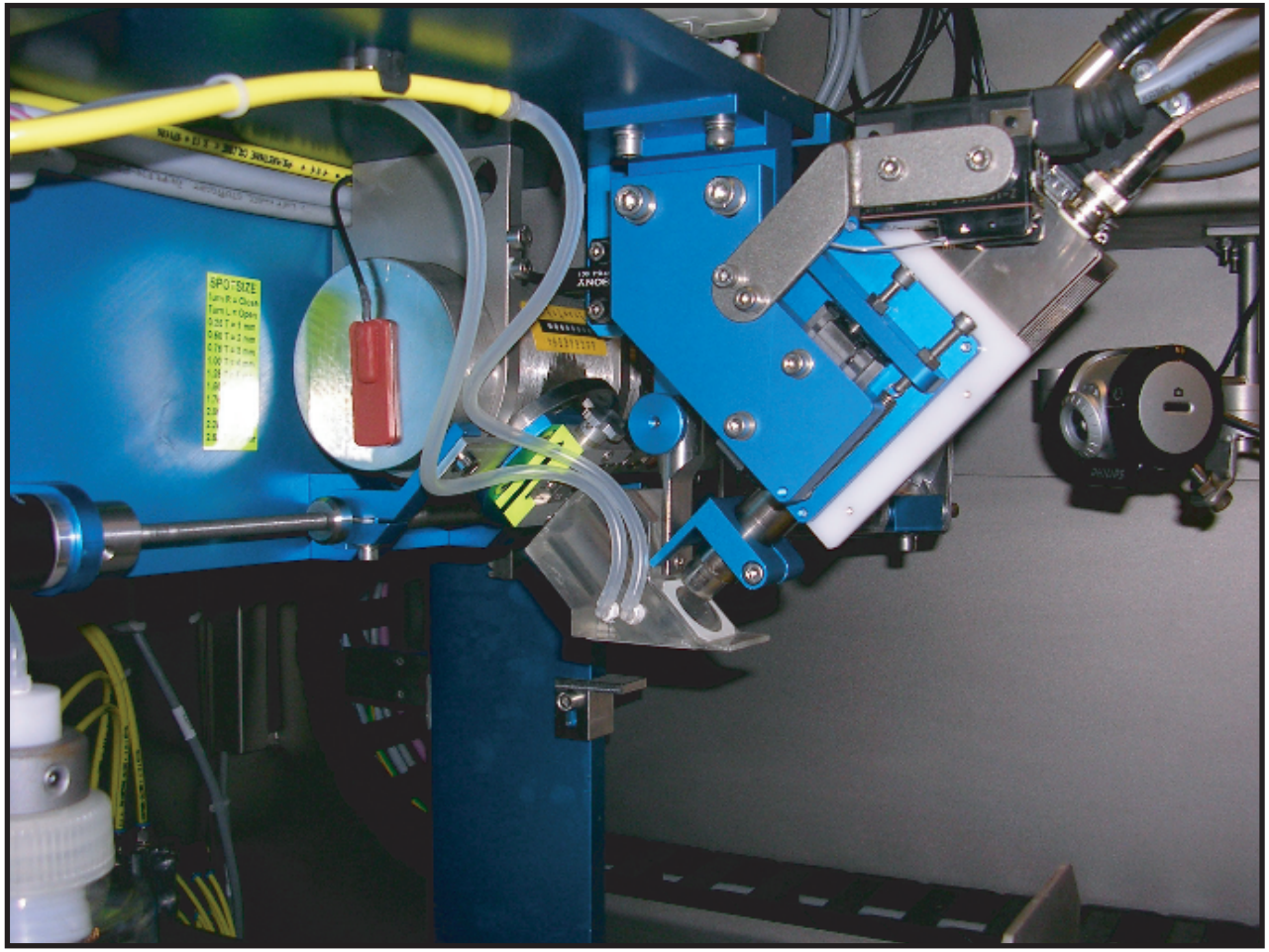

FIgure 8. Photograph of the XRF-scanner source and detector. The apparatus lands atop the sample to scan, and is incremented along the sample at the designated step size to analyze the sample.

to determine the elements present in the sample (Jenkins, 1999). The Avaatech XRF-scanner can detect elements from aluminum to uranium, and a variety of filters can be used to better detect elements of interest. This XRF-scanning technique provides the opportunity to develop continuous records of the detrital, biogenic, and redox proxies present in the tidal rhythmite.

### 2.3.1 Advanced Spectral Methods

Once a continuous geochemical proxy record has been obtained via XRF scanning, a range of advanced spectral methods can be applied to evaluate potential cyclic signals. First, Evolutive Harmonic Analysis (EHA) is used to examine the temporal stability of periodic components, and yields important insights into potential sedimentary distortions (sedimentation rate change, hiatus; Meyers et al., 2001). This time-frequency approach resolves the raw XRF data into discrete sinusoidal components of varying frequency, amplitude and phase. The observed harmonic components can then be used to evaluate specific tidal and climatic forcings present in the data (Meyers et al., 2001; Mazumder and Arima, 2004).

More specifically, the EHA technique uses Thomson's (1982) multi-taper method (MTM) spectral analysis, applied to a data window that is sequentially shifted through the study interval. The MTM technique is advantageous for our tidalite research because it provides a statistical test for the presence of periodic terms (e.g., tidal cycles) embedded in noise. The specific tapering approach provides a compromise between frequency resolution, bias, and consistency (Thomson, 1982). The type and numbers of tapers used in the EHA, and the size of the moving window for the study interval, are selected for optimal time-

frequency resolution. In addition, the MTM approach allows us to estimate power spectra for the XRF data, which represents the fraction of the variance that can be attributed to each frequency component.

Coherency analysis and cross phase spectra of the XRF data are also investigated in this study. Coherency analysis estimates the correlation between two data series at discrete frequencies. Coherency values near 1 indicate that the two data series strongly covary at a particular frequency (either positively or inversely). Cross phase analysis determines the phase relationship between coherent signals. Values near $0^{o}$ indicate that the two elements are in phase, while values near $180^{o}$ indicate an inverse relationship between the two elements of interest.

### 2.4.1 Supplementary Methods: Thin Section and SEM analysis

In this study, thin sections are cut and observed under a petrographic microscope to evaluate mineralogy, using plane polar light and crossed-polar light. Thin sections of tidal rhythmites can be used for the identification of bioturbation, to investigate the presence of microfossils, and for the identification of certain minerals (e.g., quartz, pyrite, etc.). SEM analysis has also been used to aid in the identification of certain minerals, and helps distinguish mineral trends in the data. Thin sections were carbon-coated before investigation to ensure a good image of the sample. The SEM used in this study is a Cambridge/Leica Stereoscan 440 SEM with image analysis and a $4\pi$ analyzer. Energy Dispersive X-ray Spectroscopy (EDS) and Revolution software were used to create elemental phase maps and detect sedimentary pyrite.

# CHAPTER 3

# QUANTITATIVE PALEOENVIRONMENTAL ANALYSIS OF THE PRIDE SHALE RHYTHMITES

## 3.1. Introduction

This study focuses on tidal rhythmite analysis of the Mississippian Pride Shale member in southern West Virginia. Samples collected from distal (section 3.2) and proximal (section 3.3) portions of the Pride Shale prodelta (Figure 9) are analyzed using XRF scanning, to develop continuous high-resolution paleoenvironmental proxy records. These records are analyzed using advanced spectral methods, to discern tidal and climatic controls on sedimentation in both distal and proximal settings, as well as locate the ideal sample site for extraction of tidal signals. Thin-section analysis and SEM analysis have been used to further evaluate the nature of the rhythmic sedimentation.

## 3.2. Analysis of the Rhythmic Sedimentation in the Distal Prodelta

To investigate the distal prodelta environment, a boulder containing rhythmic laminations was gathered from an outcropping along Old Spanishburg Road (see locality information in Appendix 1). The XRF scanner can only accommodate small sized samples, so the boulder was cut down to a 3x3x16 cm slab. The fissile nature of shale resulted in a need for an adhesive to promote cohesiveness of the sample during the sawing process. A combination of sodium silicate (The Science Company) and rubber latex mold compound (Mold Builder) was used to keep the sample from falling apart during the sawing process, by

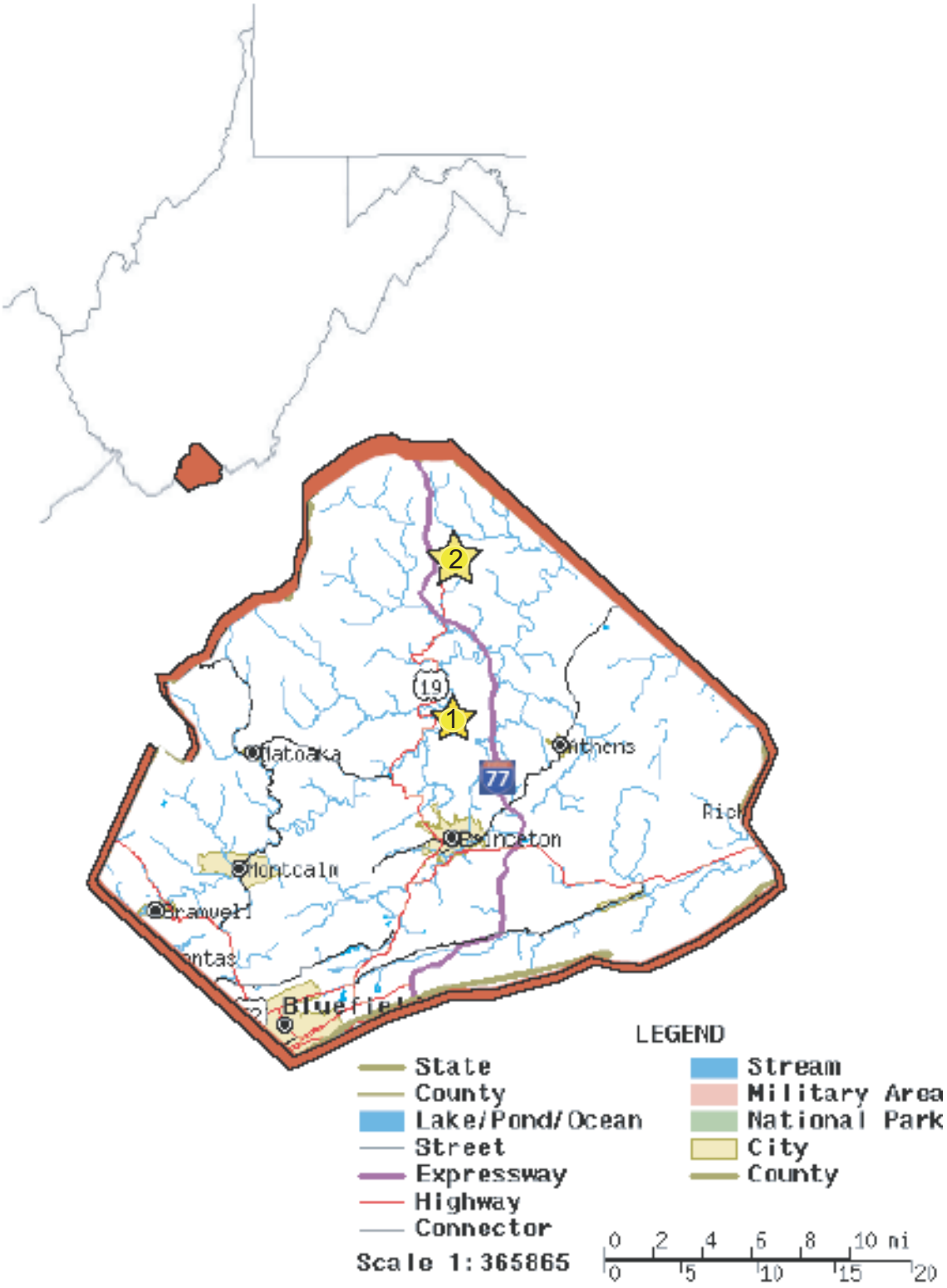


Figure 9. Location map showing the two sample sites. Location 1 is where the distal sample was taken, and Location 2 is where the proximal portion was taken. Map from www.city-data.com.

first applying layers of sodium silicate to bond the shale together, and then applying several layers of rubber mold latex compound to allow for adjustment room if the shale cracked and shifted. The analyzed portion of the slab was a clean, unpolished, horizontal surface.

### 3.2.1 Thin Section and SEM Analysis

Thin section and SEM analyses indicate that much of the sample contains angular quartz crystals with overgrowths, in addition to organic matter, clay minerals, and biotite (Figure 10). No evidence for microscopic tests or shell material was discovered. Calcium carbonate is present in the matrix, weaved throughout the sample and detected by the prominent birefringence exhibited. The calcium carbonate can be either biogenic or abiogenic, and appears to be dolomite as indicated by minimal HCl effervescence. Bioturbation is minor, however, several circular features that are in-filled with fine-grained sand are suggestive of horizontal feeding burrows. These structures are consistent with the Cruziana ichnofacies (Ekdale et al., 1984), which is typical of portions of the neritic zone where organic matter is abundant (Boggs, 1987).

### 3.2.2 XRF-Scanning Analysis

Initial XRF-scanning of the distal Pride Shale slab was conducted using a 1 mm spatial resolution: a 10kV/1000 μA scan for 30 seconds, and a 30 kV/1000 μA scan with a Pd-thin filter for 60 seconds. These parameters were chosen to ensure good detection of a broad range of elements of interest. Based on these results, more detailed analyses at 0.5 mm resolution were conducted: a 10kV/1000 μA scan for 60 seconds, and a 30 kV/1000 μA scan

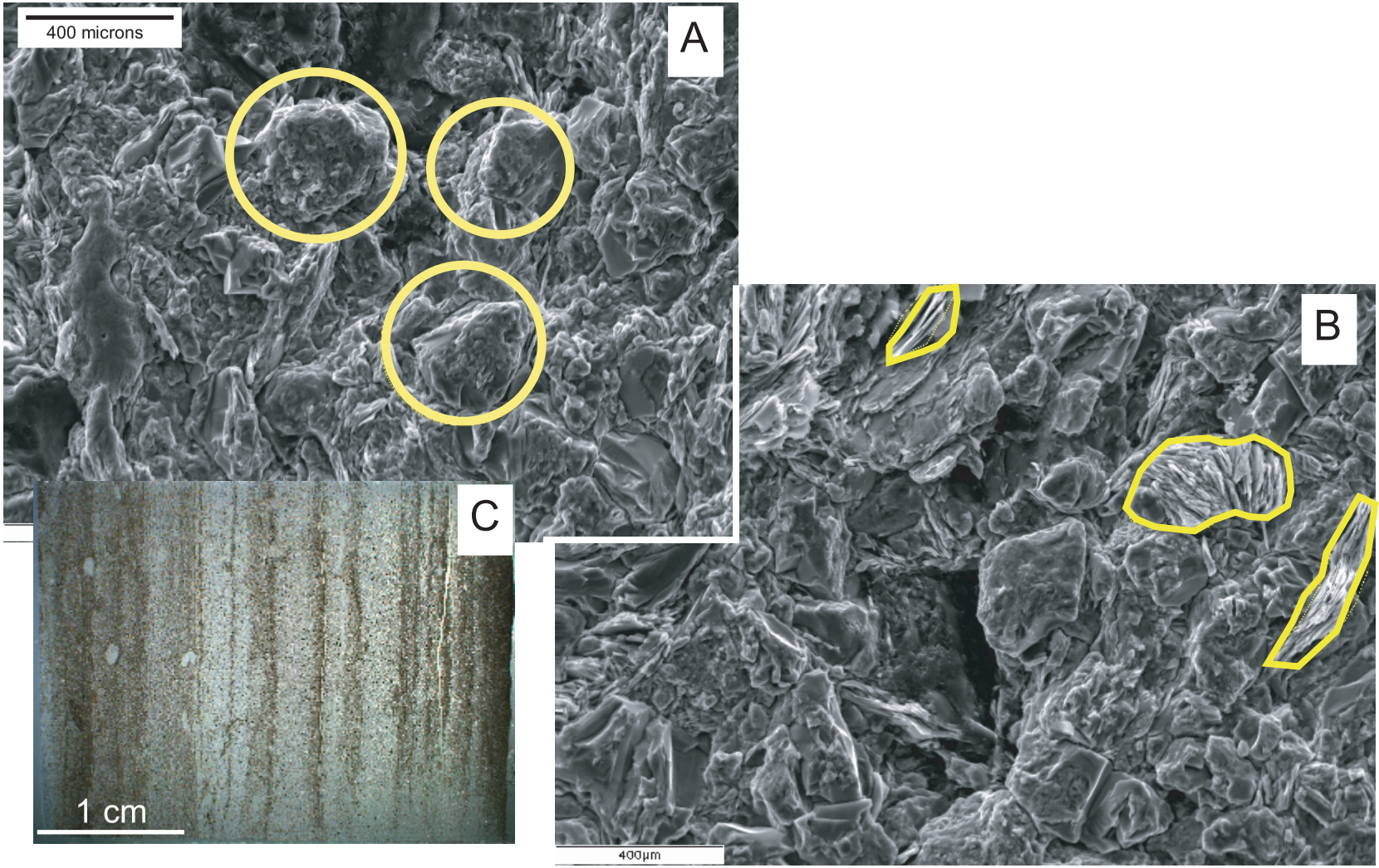


Figure 10. Angular quartz grains are identified by the yellow circles in the SEM image of Figure 10a. Note overgrowth of silica in image. Biotite is identified by yellow outlines in the SEM image of Figure 10b. A thin section image is shown in Figure 10c. Note the infrequent horizontal burrow structures.

with a Pd-thin filter for 120 seconds. The 0.5 mm resolution analysis is discussed in detail below.

After careful inspection of the 0.5mm resolution XRF-data, and comparison with the sedimentologic character of the rhythmites, three paleoenvironmental proxies were selected for advanced spectral analysis. These include titanium, silicon/titanium, and sulfur, which are proposed proxies for detrital, biogenic and authigenic processes, respectively. Each of the proxies is discussed in detail in the following sections.

#### 3.2.2.1 Detritial and Biogenic Proxies

In the Pride Shale slab, a wide range of elements commonly associated with detritial siliciclastic minerals show strong covariance with titanium (Fe, K, Al, etc.; Figure 11; Sageman and Lyons, 2004). For example, the linear relationship between titanium and iron indicates that most of the iron in the sample is derived from detrital sources (Figure 12). Darker laminations within the Pride Shale sample contain increased amounts of titanium, indicating greater terrigenous silt contribution, as well as increased amounts of detrital iron, potassium, aluminum and rubidium (Figures 11 and 13).

In sharp contrast to most of the detrital elements (Figure 11), silicon and calcium display a general inverse correlation to titanium, with the exception of a few outliers attributable to minor cracks in the Pride Shale slab (Figure 14). This inverse correlation suggests an alternate source for most of the silicon and calcium, and a possible candidate is a biogenic skeletal contribution. Given this assumption we employ the Si/Ti ratio to evaluate change in the amount of biogenic silica.

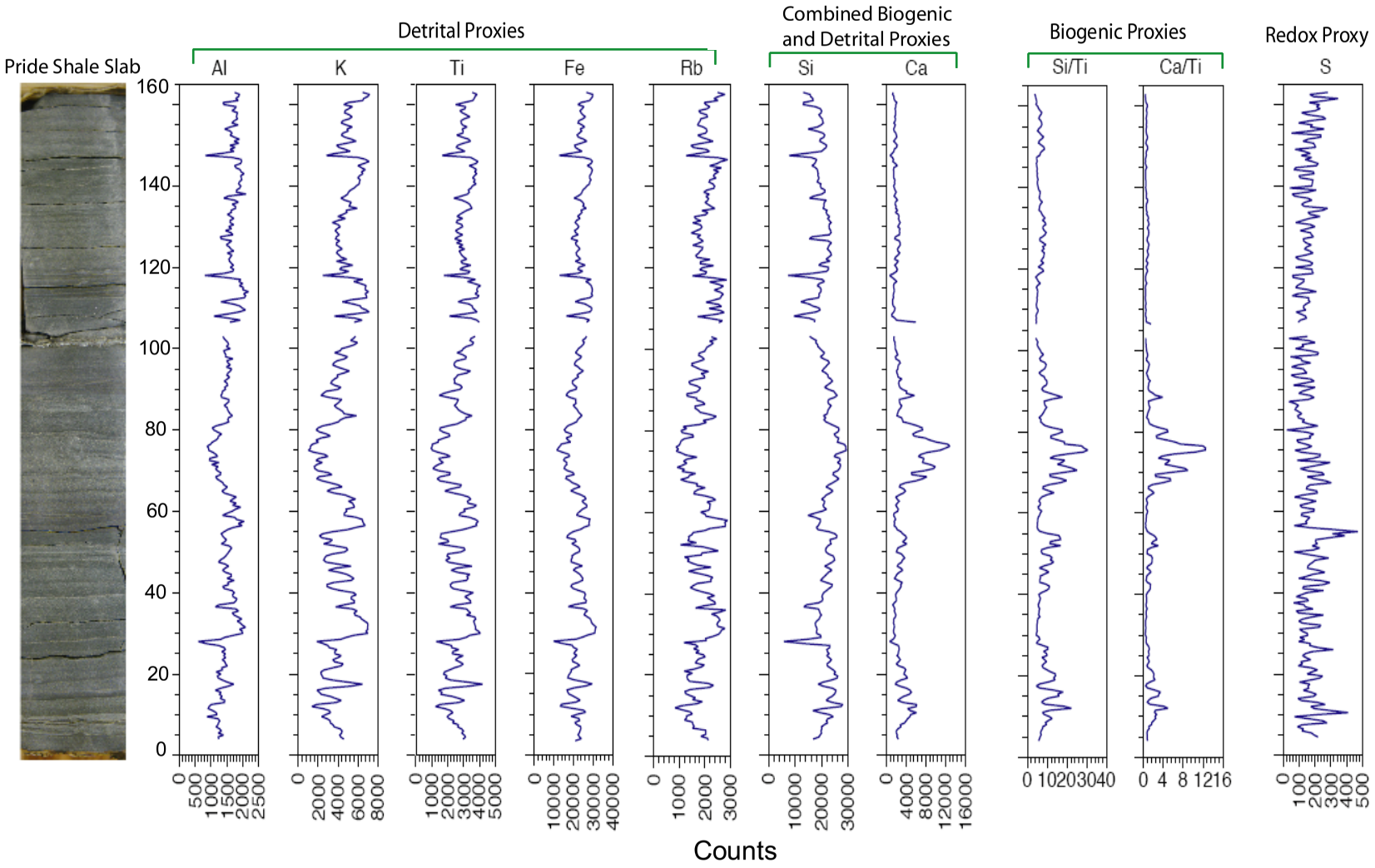


Figure 11. XRF-scanning results for the distal Pride Shale sample, alongside a photograph of the analyzed interval. Select detrital, biogenic, and redox proxies are displayed. All results are expressed as XRF counts. Height axis is in millimeters.

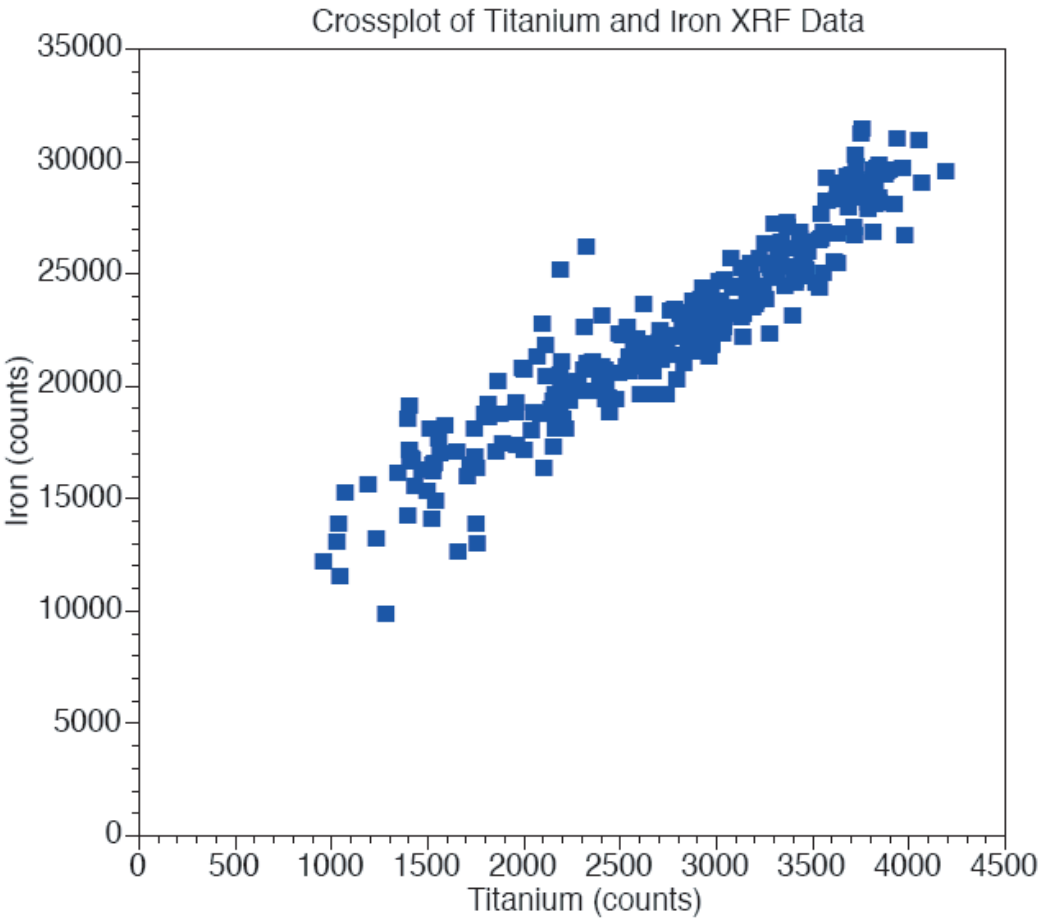


Figure 12. Crossplot of titanium and iron XRF counts from the distal Pride Shale sample. These two elements show strong covariation, and are most likely due to terrigenous sources.

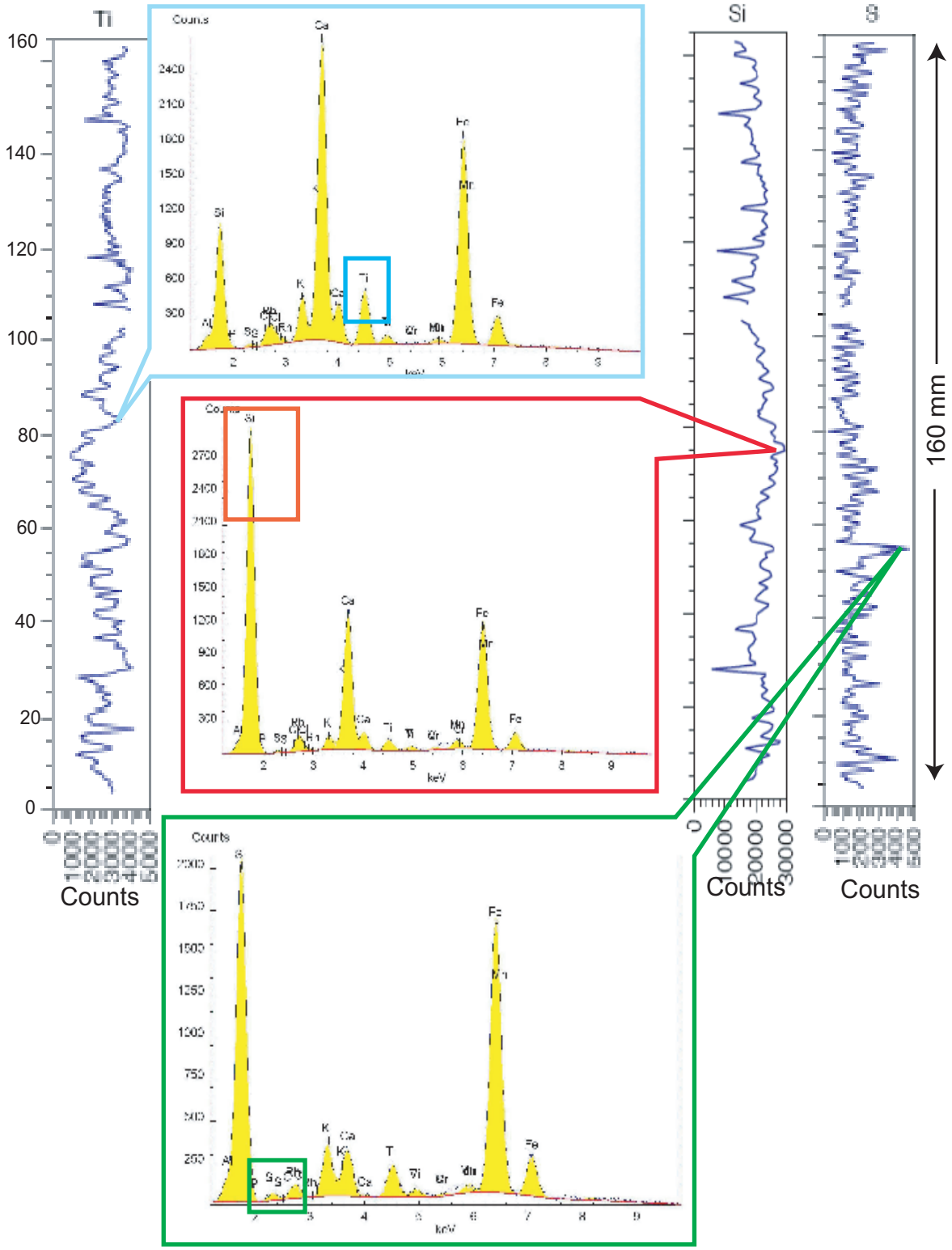


Figure 13. XRF spectra for select samples from the distal Pride Shale sample, illustrating the quality of the data.

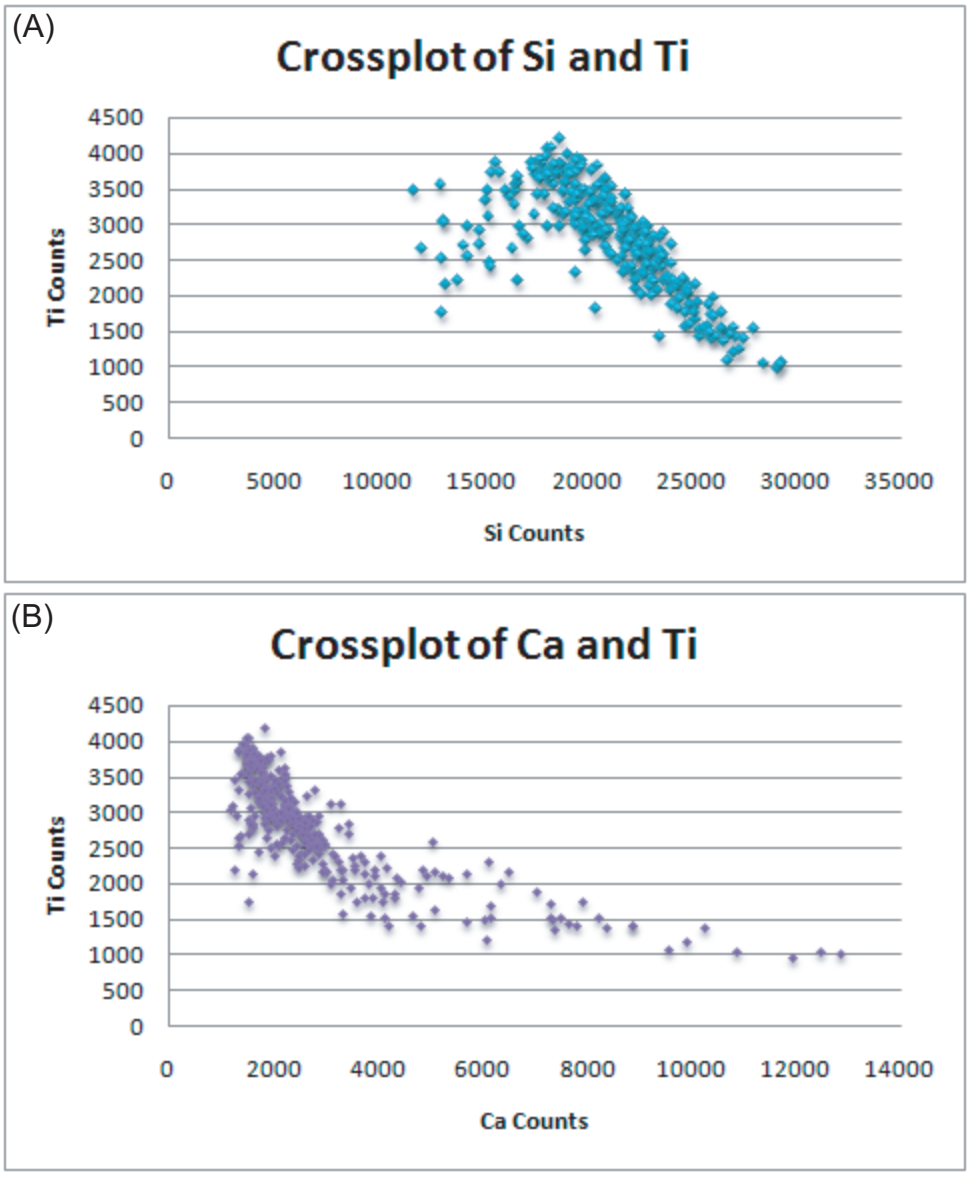


Figure 14. (A) Crossplot of the silicon and titanium XRF counts from the distal Pride Shale sample. (B) Crossplot of the calcium and titanium XRF counts from the distal Pride Shale sample. Figures 14A and 14B show primarily negative correlations (with the exception of a few outliers attributable to minor cracks in the Pride Shale slab), possibly indicating biogenic sources for both the silicon and calcium.

Use of the silicon/titanium ratio allows us to identify increases and decreases in silica that are not coupled to changes in detrital flux. Silicon/titanium values increase in the lighter colored laminations and decrease in darker laminations (Figure 11). This same trend is observed in calcium/titanium values, which can be interpreted as a proxy for biogenic calcium carbonate (Figure 11). Our results suggest that both biogenic silica and biogenic calcium carbonate are elevated in the lighter colored laminations. As noted above, the presence of calcite/dolomite in these light layers has been confirmed via thin section analysis.

While we can interpret the Si/Ti and Ca/Ti ratios as representative of changes in biogenic skeletal contribution, an alternate hypothesis is that increases in these ratios actually reflect an increased detrital quartz sand contribution, and an associated increase in calcite cement within the matrix. If this were true, variability in the Si/Ti ratio would indicate changes in the relative contribution of sand versus silt-sized sediment. In fact, it is difficult to evaluate which of the two hypothesis is correct based on available geochemical and sedimentologic data from the Pride Shale slab. In the analysis presented below, we will infer a biogenic origin for the Si/Ti variability, and we will further test this hypothesis by comparing our results from proximal and distal basin sites (see section 3.3.1).

#### 3.2.2.2 Authigenic Proxy

In contrast to the XRF data discussed so far, total sulfur shows no obvious consistent relationship with laminae color (Figures 11 and 13). Scanning Electron Microscope (SEM) imaging was used to further evaluate the distribution of sulfur in the sample (Figure 15). A detailed elemental map of the thin section, constructed using EDS (Energy Dispersive Spectrometry), shows the abundance of sulfur across multiple laminations. Variability in the

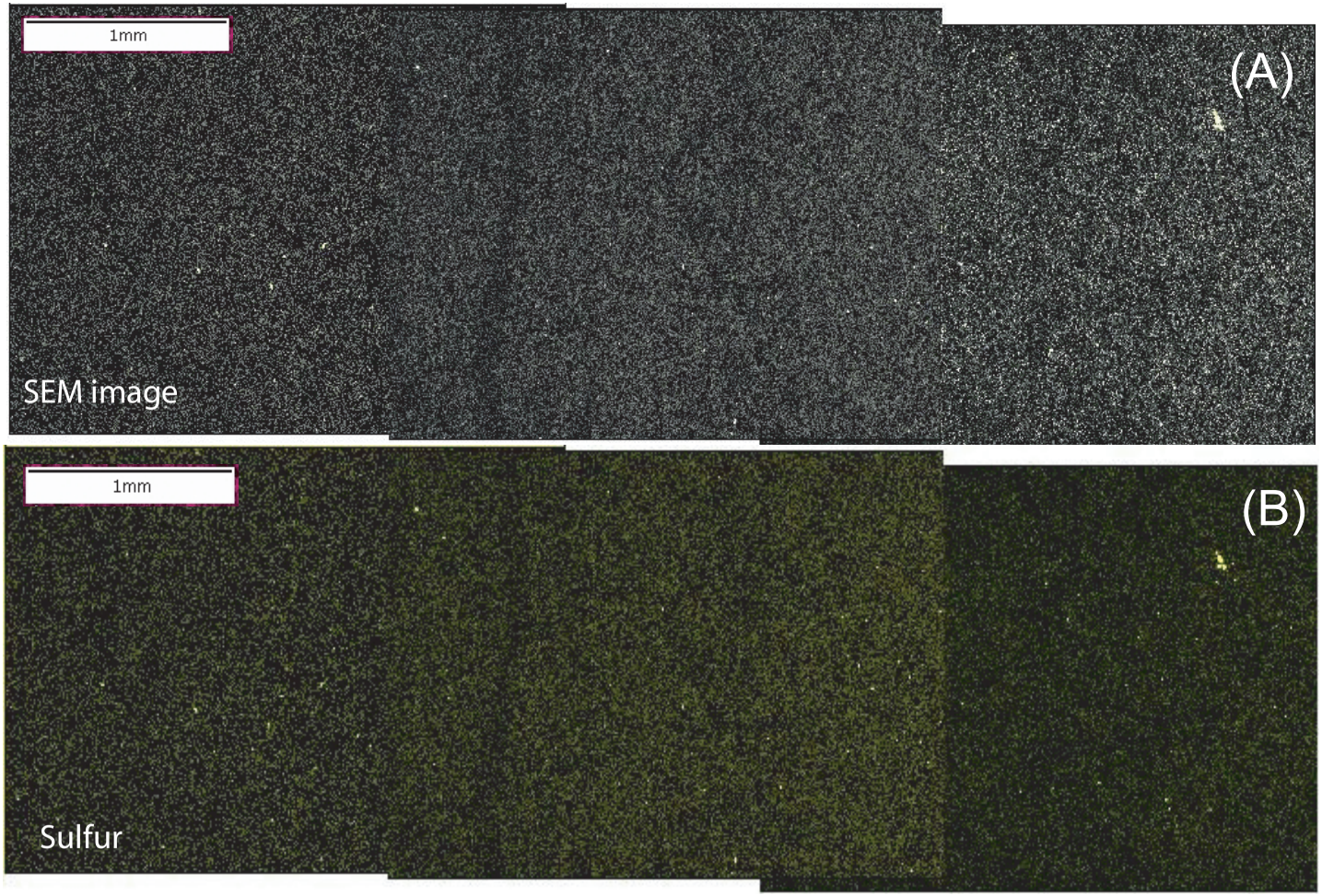


Figure 15. SEM Image of thin section from the distal Pride Shale sample, showing the raw SEM (A) and the elemental phase map for sulfur (B).

abundance of sulfur across the image is evaluated using the software ImageJ (a free program by W. Rasband) to quantify color changes in the elemental map (Figure 16). Comparison of the ImageJ results and the XRF-scanner sulfur data demonstrates that the two plots show similar trends. Based on this analysis, it is clear that the XRF-scanner sulfur data is integrating changes in the abundance of widely distributed disseminated pyrite across 0.5 mm intervals, and there is no evidence for discrete pyritized layers.

### 3.2.3 Evolutive Harmonic Analysis

The titanium, silicon/titanium and sulfur XRF data have been analyzed using Evolutive Harmonic Analysis (Thomson, 1982; Meyers et al., 2001). All analyses employed three $2\pi$ data tapers. Evolutive Harmonic Analysis utilized a 50 mm moving window with a 1 mm increment.

Evolutive Harmonic Analyses of the distal Pride Shale titanium data and silicon/titanium data (Figure 17 and 18) reveal a dominant high amplitude cycle with a period of approximately 27 mm. This cycle is persistent throughout most of the 16 cm slab, although its amplitude is variable, with highest amplitude in the middle portion. A bifurcation of the 27 mm period at ~90 mm height may indicate the presence of a hiatus (Meyers et al., 2001; Meyers and Sageman, 2004). However, throughout most of the tidalite, sedimentation appears to have been remarkably steady, a conclusion that is further supported by only minor frequency drift in the relatively persistent shorter period components (e.g., the 8.47 mm period in Figure 17 and 18).

Comparison of the EHA results with amplitude and power spectra of the entire data sets confirms the presence of an ~27 mm period, which is characterized by a significant

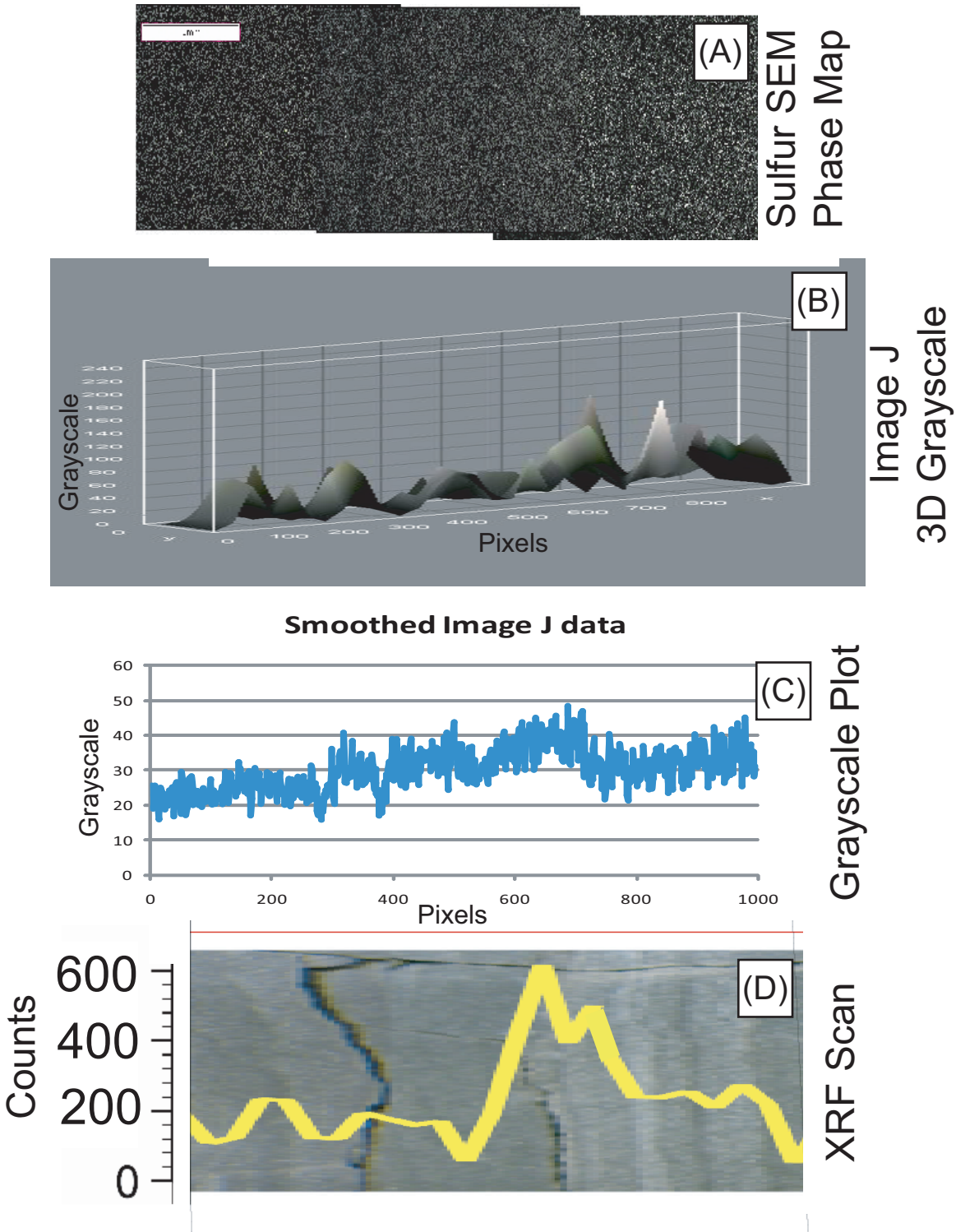


Figure 16. (A) SEM phase map of sulfur (B) 3D volume calculation of grayscale value for the image in 16A. (C) Smoothed grayscale value for the image in 16A. (D) Sulfur XRF-scanning results for approximately the same interval of the Pride Shale sample.

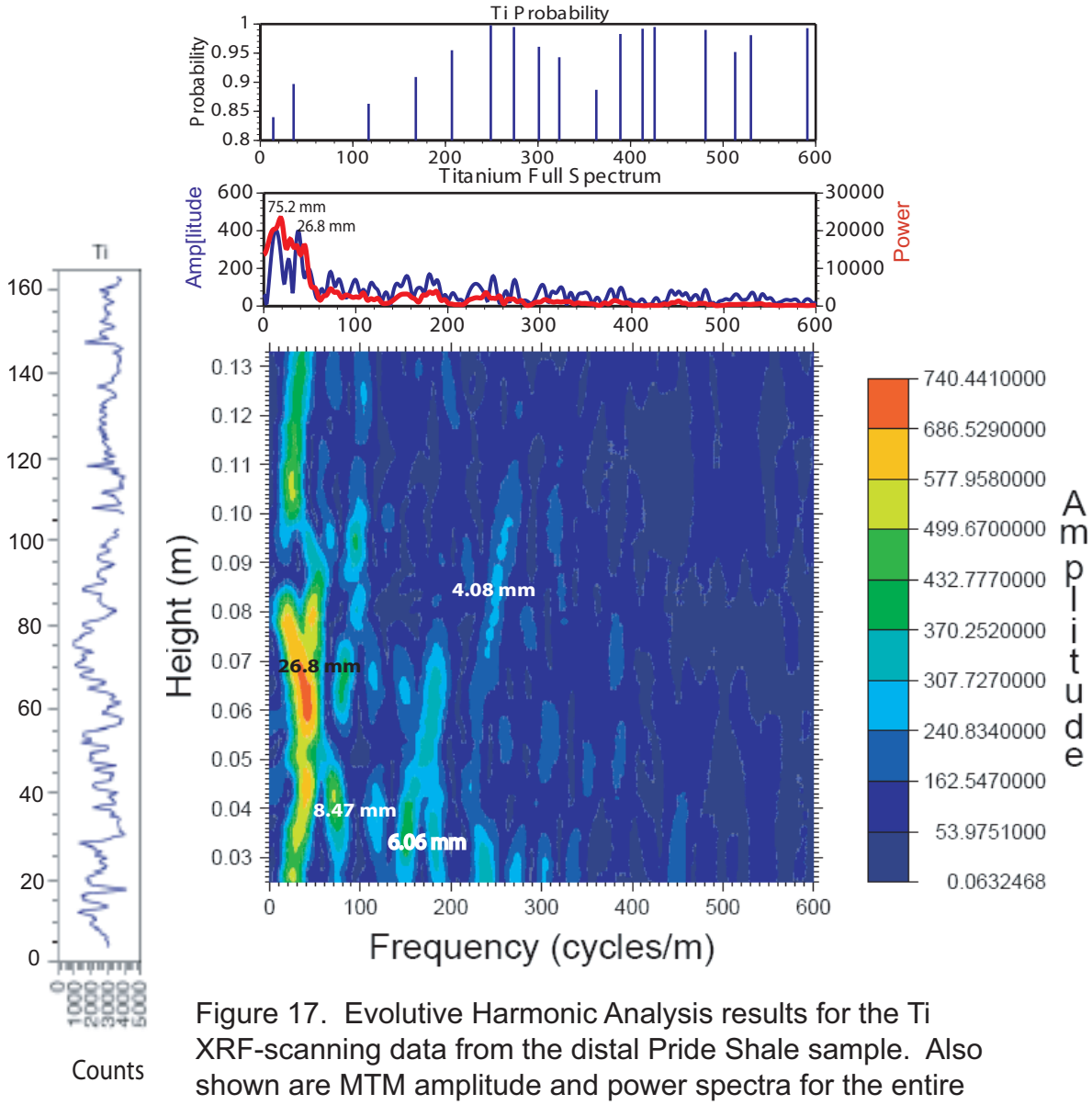


Figure 17. Evolutive Harmonic Analysis results for the Ti XRF-scanning data from the distal Pride Shale sample. Also shown are MTM amplitude and power spectra for the entire data set, as well as probability results from the MTM harmonic test.

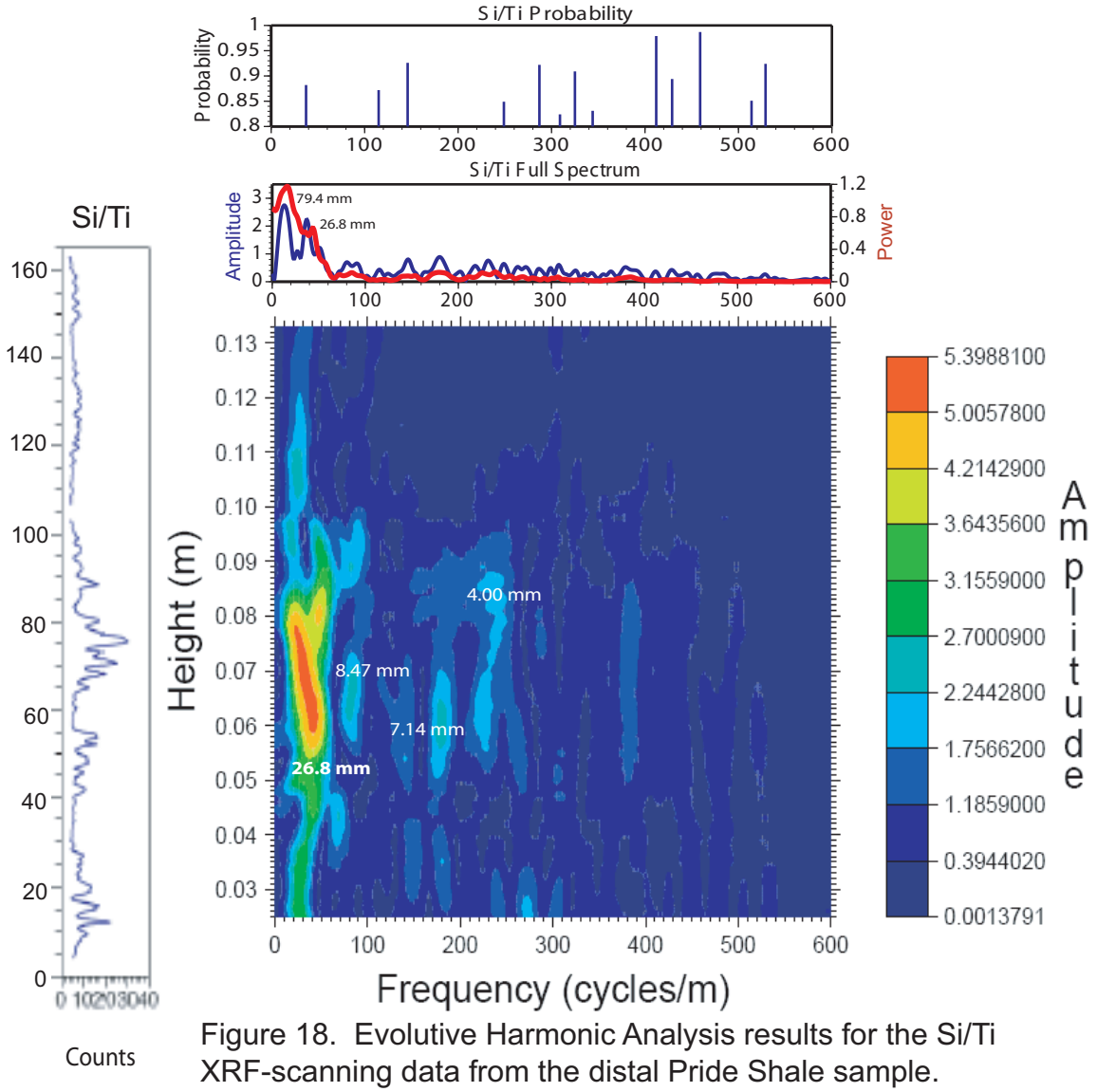


Figure 18. Evolutive Harmonic Analysis results for the Si/Ti XRF-scanning data from the distal Pride Shale sample. Also shown are MTM amplitude and power spectra for the entire data set, as well as probability results from the MTM harmonic test.

harmonic probability (top of Figure 13, top of Figure 16.). The analysis also reveals a longer period cycle of approximately 75 mm, or nearly half of the 160 mm slab. However, this period is only significant in the Ti XRF data. Table 1 summarizes the results from our analysis, indicating all relatively persistent tidalite periods.

In contrast to the results for Ti and Si/Ti, Evolutive Harmonic Analysis of the sulfur data (Figure 19) reveals a dominant cyclicity of 2.27 mm. This cyclicity is fairly stable and persistent throughout the slab. This observation further supports the hypothesis of relatively steady sedimentation during the deposition of this tidalite, although minor disturbances are apparent. Additional lower frequency cycles are also observed in the sulfur data, some of which are similar to the Si/Ti and Ti EHA results. These periods are summarized in Table 1. The relationship between the prominent frequencies observed in the titanium, silicon/titanium, and sulfur data will be further explored using coherency and cross-phase analysis.

### 3.2.4 Coherency and Cross-Phase Analysis

Coherency and cross-phase spectral analysis of the Pride Shale titanium (detrital proxy), silicon/titanium (biogenic proxy) and sufur (redox proxy) data is presented. All data were analyzed using multi-taper method spectral analysis, with three $2\pi$ data tapers (Thomson, 1982). The Si/Ti and Ti data (Figure 20) are generally antiphased at low frequencies, with a drift towards in-phase variability at higher frequencies. The records indicate strong coherence at each of the dominant frequencies identified in Figures 17 and 18, while the results for sulfur vs. silicon/titanium, and sulfur vs. titanium, show more complicated spectra (Figures 21 and 22).

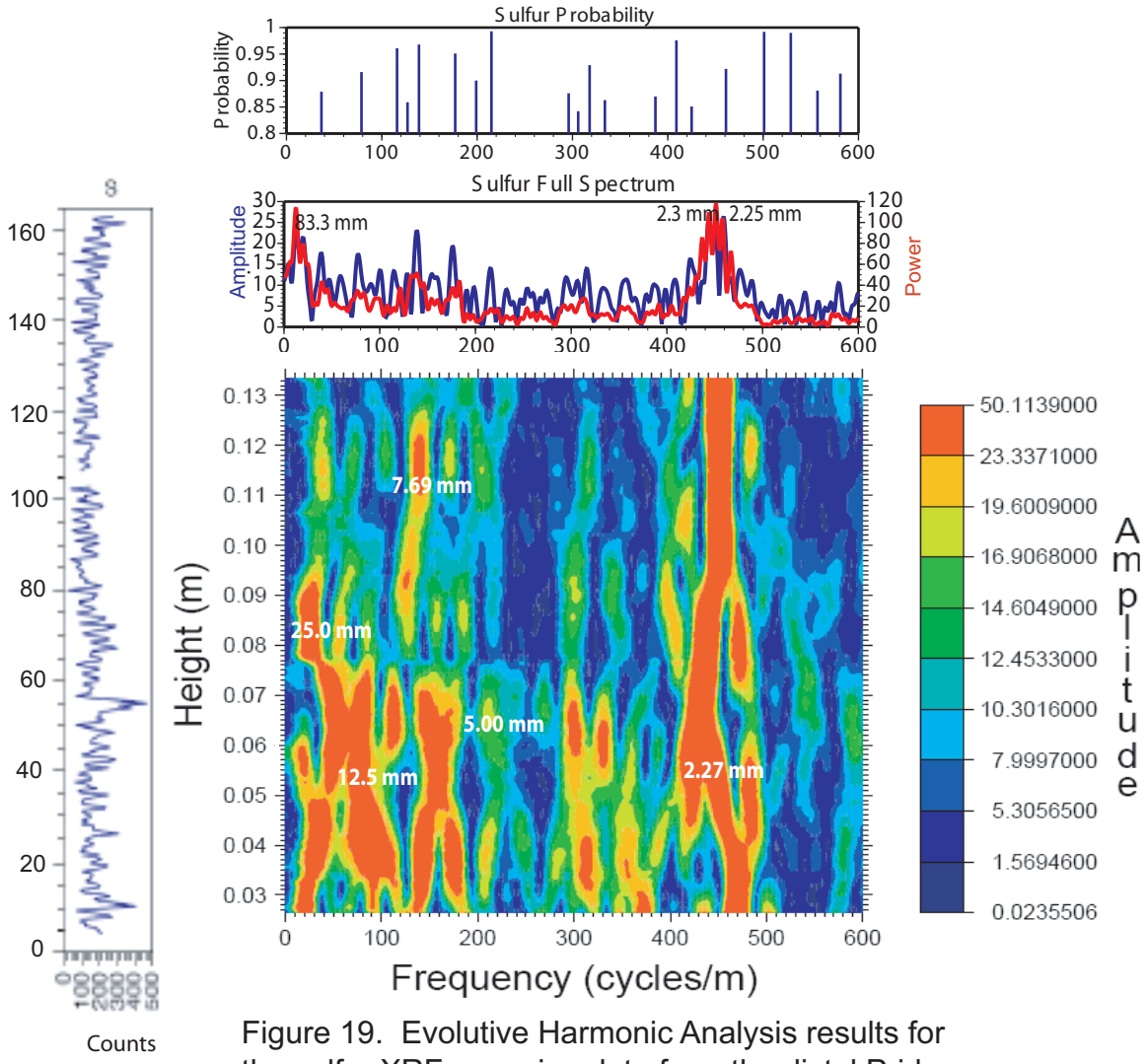


Figure 19. Evolutive Harmonic Analysis results for the sulfur XRF-scanning data from the distal Pride Shale sample. Also shown are MTM amplitude and power spectra for the entire data set, as well as probability results from the MTM harmonic test.

| Element | Spatial Period |
|---|---|
| Ti | 26.8 mm |
| | 8.47 mm |
| | 6.06 mm |
| | 4.08 mm |
| Si/Ti | 26.8 mm |
| | 8.47 mm |
| | 7.14 mm |
| | 4.00 mm |
| S | 25.0 mm |
| | 12.5 mm |
| | 7.69 mm |
| | 5.00 mm |
| | 2.27 mm |

Table 1. Observed spatial periods in the distal Pride Shale sample.

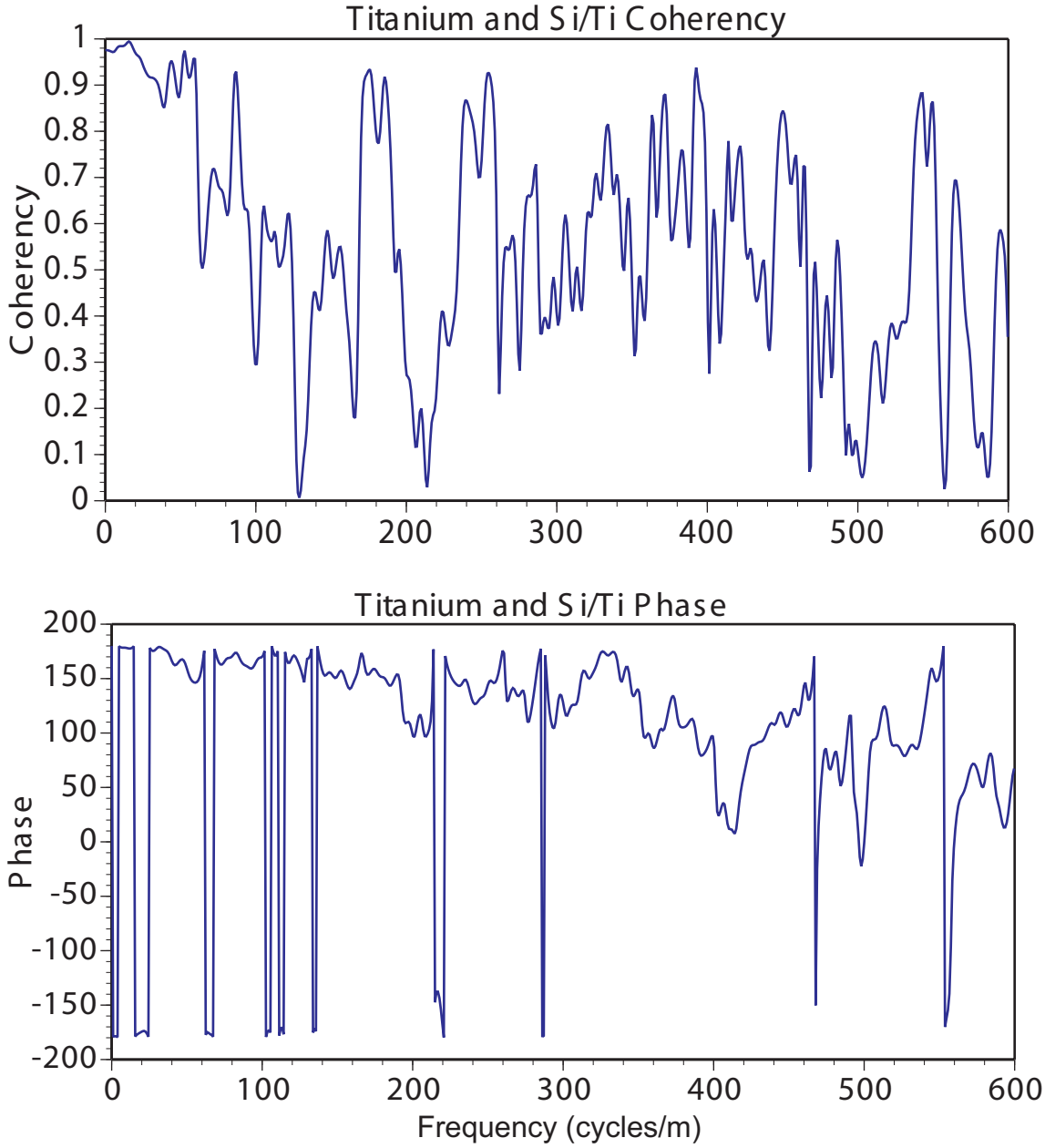


Figure 20. MTM coherency and cross phase analysis for titanium and Si/Ti XRF-scanner data from the distal Pride Shale sample.

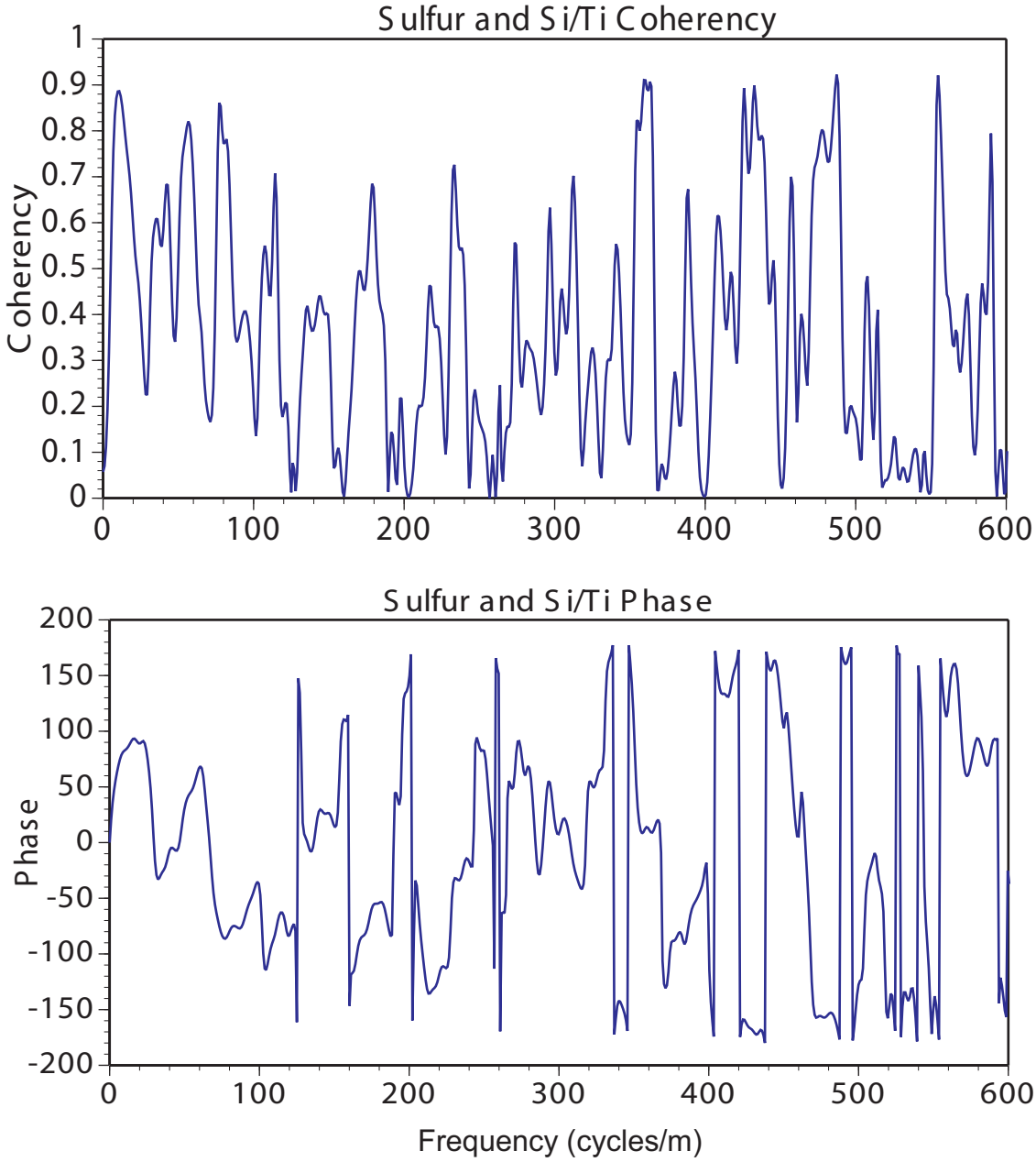


Figure 21. MTM coherency and cross phase analysis for sulfur and Si/Ti XRF-scanner data from the distal Pride Shale sample.

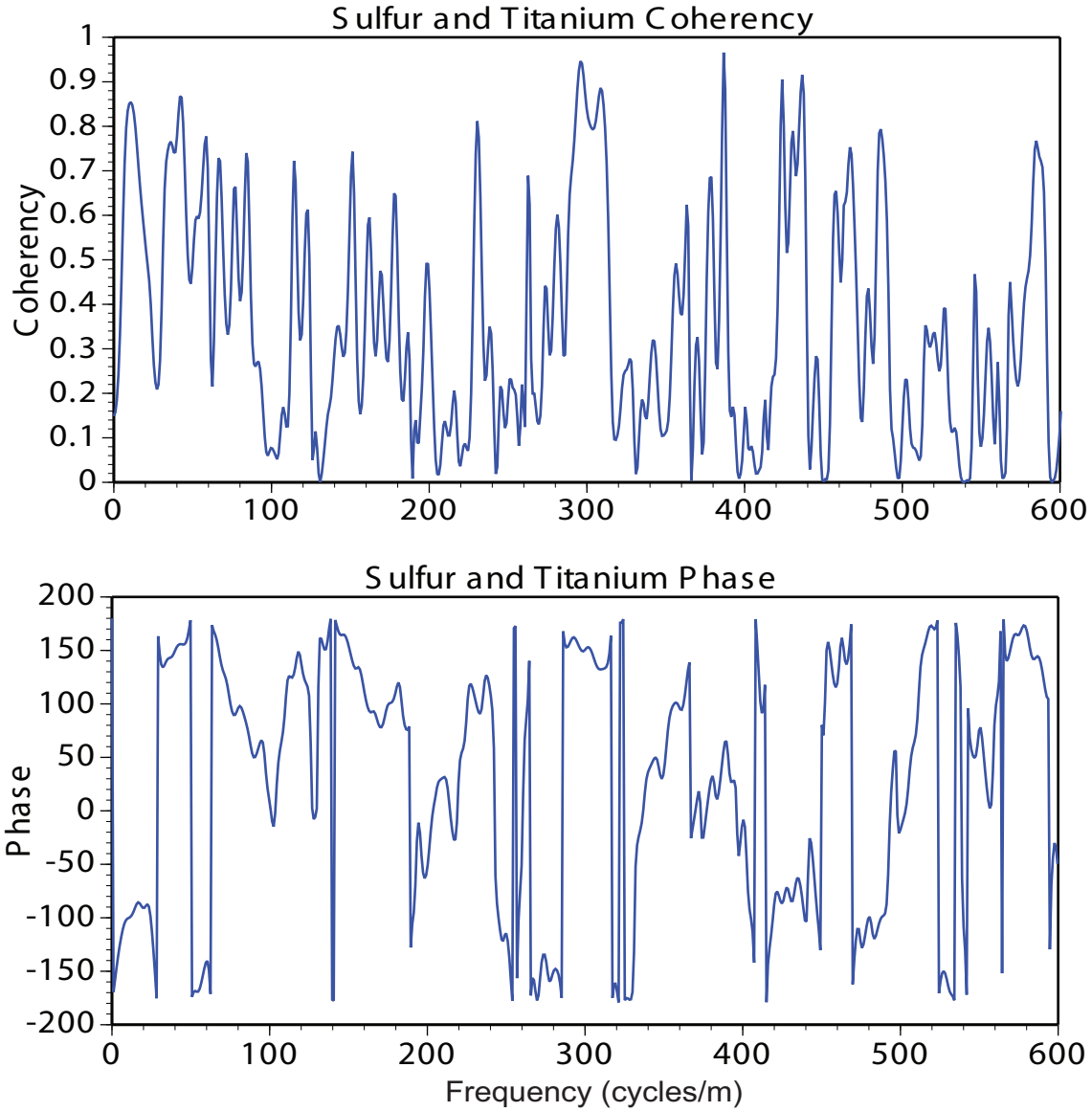


Figure 22. MTM coherency and cross phase analysis for titanium and sulfur XRF-scanning data from the distal Pride Shale sample.

### 3.2.5 Discussion

The two most dominant periodic periods observed in our analysis include an ~27 mm cycle (Ti,Si/Ti, S), and an ~2.27 mm cycle (S). We will focus our discussion on these two prominent cycles, and attempt to develop a depositional model to account for their presence. First, based on the 1:12 relationship between these two dominant periods, we hypothesize that the ~27 mm cycles represents an annual cycle, while the ~2.27 mm cycle represents a monthly tidal rhythm.

#### 3.2.5.1 The hypothesized annual Ti and Si/Ti rhythm

One possible source of the strong ~27 mm period that is highly coherent and anti-phased in the titanium and silicon/titanium is an annual change in detrital versus biogenic flux to the sediment. For example, this type of synchronized anti-phased variability is observed in the modern day Cariaco Basin, due to migration of the Intertropical Convergence Zone (Haug et al., 2001). The Cariaco Basin is located at a latitude of 10° south in Venezuela, and records increased detritus flux when the ITCZ is directly overhead; when the ITCZ is further south, sedimentation dominantly consists of siliceous oozes and organic matter (Haug et al, 2001). Since the Pride Shale is located at a similar paleolatitude as the modern Cariaco Basin (Figure 23), the ~27 mm cycle observed in the Pride Shale may be recording the annual migration of the ITCZ during the Mississippian.

Another modern analogue for this type of inversely related detrital and biogenic flux is the prodeltaic facies of the late Miocene Amazon River basin. Studies of the tide-dominated delta system identified semi-diurnal, fortnightly, and seasonal controls on

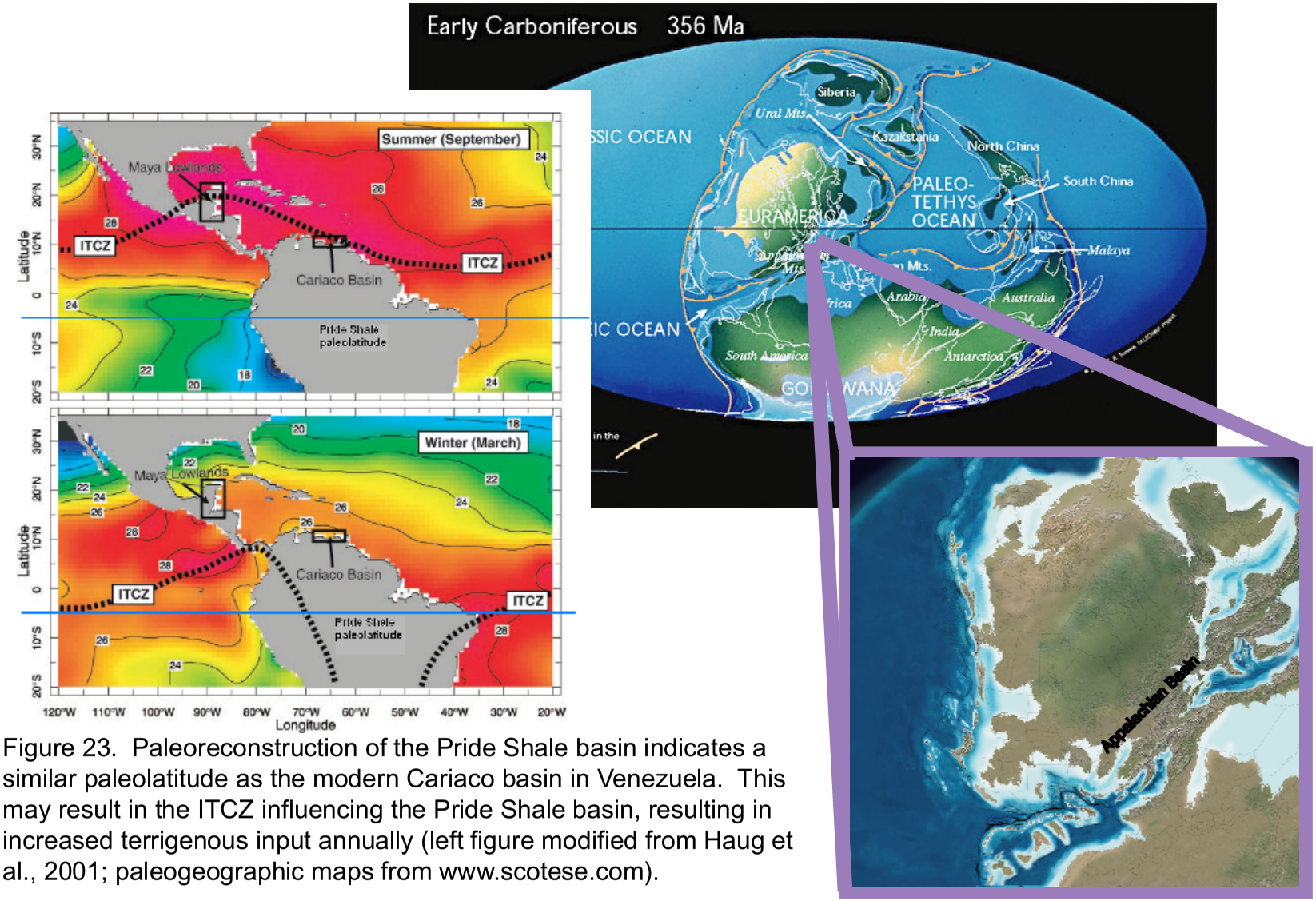


Figure 23. Paleoreconstruction of the Pride Shale basin indicates a similar paleolatitude as the modern Cariaco basin in Venezuela. This may result in the ITCZ influencing the Pride Shale basin, resulting in increased terrigenous input annually (left figure modified from Haug et al., 2001; paleogeographic maps from www.scotese.com).

deposition based on sedimentological observations, which were quantified using Fourier Analysis (Hovikoski et al., 2008). An annual cycle was recorded in the tidalite, and interpreted as a result of ITCZ migration over the basin (Hovikoski et al., 2008)

Alternatively, the observed ~27 mm cycle may be associated with the annual summer monsoon. The summer monsoon occurs when the land is hot relative to the cool ocean; low air pressure over the land results in precipitation on the land, with increased detritus input into a sedimentary basin, due to increased runoff (Ruddiman, 2001). The large landmass present during the Mississippian may have allowed for a heightened monsoonal signal over the Pride Shale basin, resulting in increased precipitation during the monsoon season and biogenic sedimentation the rest of the year.

In order to discern between the ITCZ and summer monsoon, a better sample of the Pride Shale is needed. The ideal sample would contain a daily signal, so that one could count the number of days in a year during the Mississippian, as well as still contain the annual climatic cycle. Once laminae associated with individual days are identified, we can potentially count the number of days elapsed, to determine whether the increase in detrital input occurs during the peak of the summer monsoon, or alternatively, when the ITCZ is overhead.

Finally, if the Si/Ti variation is attributable to grain size variation rather than changes in biogenic silica contribution, the observed anti-phased 27 mm cycle in Ti and Si/Ti could also be climatic in nature. In this case, coarser grained sediment should be deposited when the ITCZ is overhead, or during the summer monsoon season. The increase of detrital sediment flux into the system during this time would produce coarser-grained sediment on

the prodelta, resulting in an increased Si/Ti ratio. Finer-grained sediment associated with decreased silicon (quartz) flux would be deposited the remainder of the year.

#### 3.2.5.2 The hypothesized monthly sulfur rhythm

To understand the origin of a monthly sulfur tidal signature, a semi-monthly signal is explored. Semi-monthly neap-spring tides are produced by the alignment of the earth-moon-sun system (Figure 24); if all three elements are aligned, spring tides (higher magnitude tides) are produced, while neap tides are produced when the moon is at a right angle to the earth and sun (Kvale, 2006). However, the elliptical orbit of the moon causes unequal magnitude spring tides (Figure 24), with one high spring tide, and one low spring tide; the period of time from one high spring tide to the next is the anomalistic month (Frouin et al., 2006).

Our observation of a monthly tidal cycle in the sulfur data may be a consequence of sedimentation during high spring tides. If increased marine organic matter concentration within the sediments is associated with higher seal level during spring tidies, higher rates of sulfate reduction could produce more hydrogen sulfide. A second hypothesis for a monthly authigenic sulfur signal is related to the current strength in the depositional system. Monthly low neap tides may result in enhanced winnowing of less dense material due to an increased current strength, resulting in a lag of pyrite.

A modern analog for a monthly tidal signature is the Amazon River Basin. The Amazon River basin deltaic facies show distinct thickening and thinning of laminations, which is interpreted to represent the monthly apogean-perigean relationship (Hovikoski et al., 2008); the sediment also contains pyrite produced by hydrogen sulfide reacting with iron.

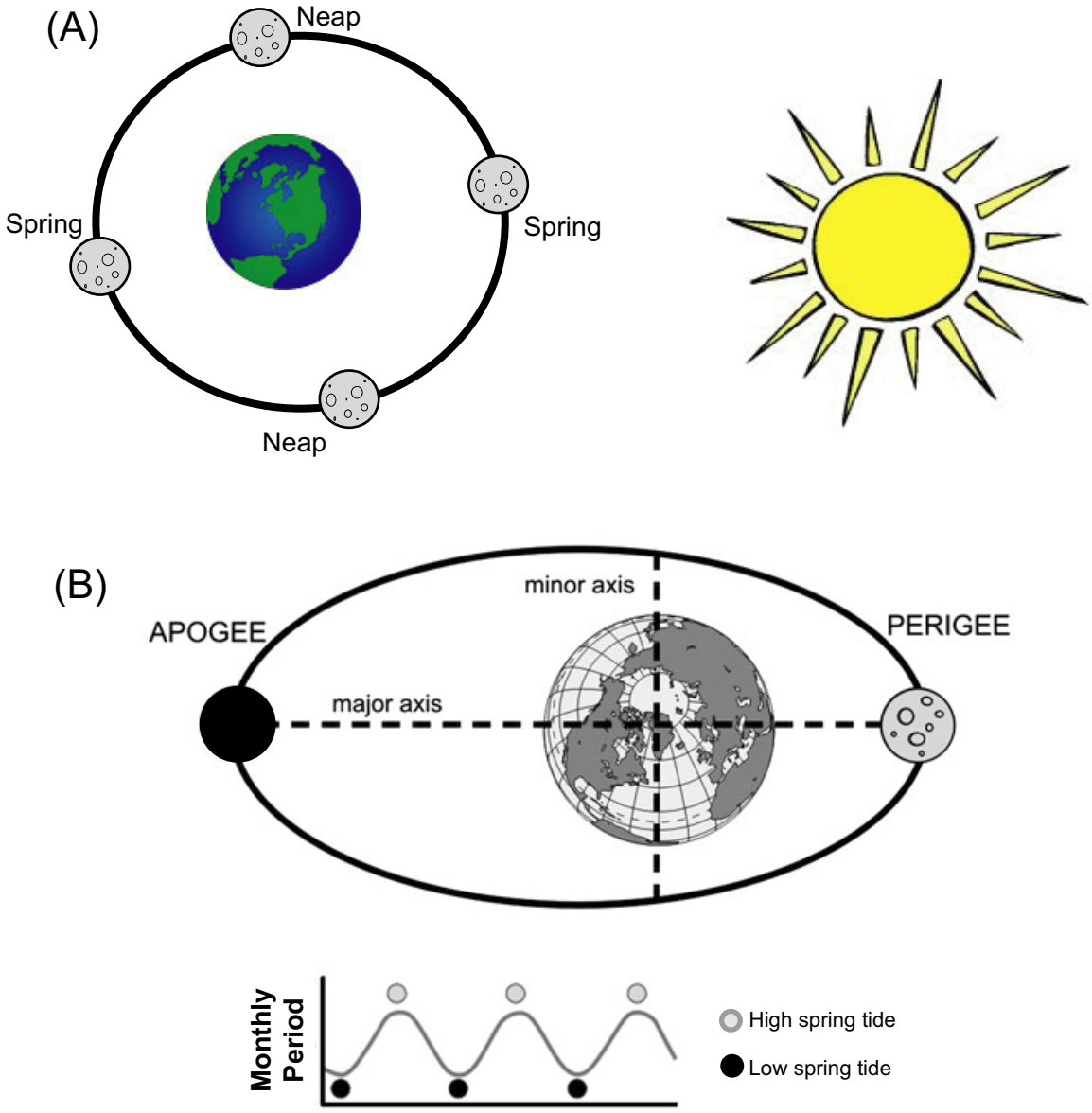


Figure 24. Neap-spring tides (A) produce semi-monthly signatures based on the rotation of the moon around the earth. Spring tides are produced when the earth-moon-sun system is aligned. The elliptical shape of the moon's orbit around the earth (B) produces two different magnitude spring tides. The time it takes to go from one high spring tide to the next produces a monthly tidal signature (modified from Frouin et al., 2006).

### 3.2.5.3 A Summary of our Preferred Model for Deposition

Our complete model for the interpretation of each elemental proxy is shown in Figure 25. The Ti detrital proxy is elevated during times of increased precipitation, either due to an annual ITCZ or monsoonal influence, which results in enhanced terrigenous sedimentation. The biogenic Si/Ti proxy is elevated during times of seasonally increased biogenic silica productivity in the overlying water column. On a monthly cycle, elevated sulfide content with the sediments occurs due to an increase in marine organic matter content in the surface sediments, and enhanced sulfate reduction, associated with high spring tides. Alternatively, the concentration of disseminated pyrite increases every month due to winnowing from a more vigorous low neap tide current strength.

## 3.3 Analysis of the Rhythmic Sedimentation in the Proximal Prodelta

Additional field work along Interstate 77 at Exit 20 in Camp Creek (Locality Description in Appendix 1; Figures 9 and 26) provided the opportunity to obtain a sample from a more proximal portion of the Pride prodelta, to compare with previous analyses of the more distal prodelta (as discussed above). A large slab was excavated from the outcrop using a concrete saw. Sodium silicate (The Science Company) and rubber latex mold (Mold Builder) were applied to the outcrop (Figure 27), with foam sealant (Handi-Foam) coating the sample area for protection.

Visual observations indicate that the laminations present in the Interstate 77 slab are not as prominent as the laminations in the distal prodelta sample. As will be demonstrated, the poorer character of the rhythmic signature indicates that sampling area must be optimized

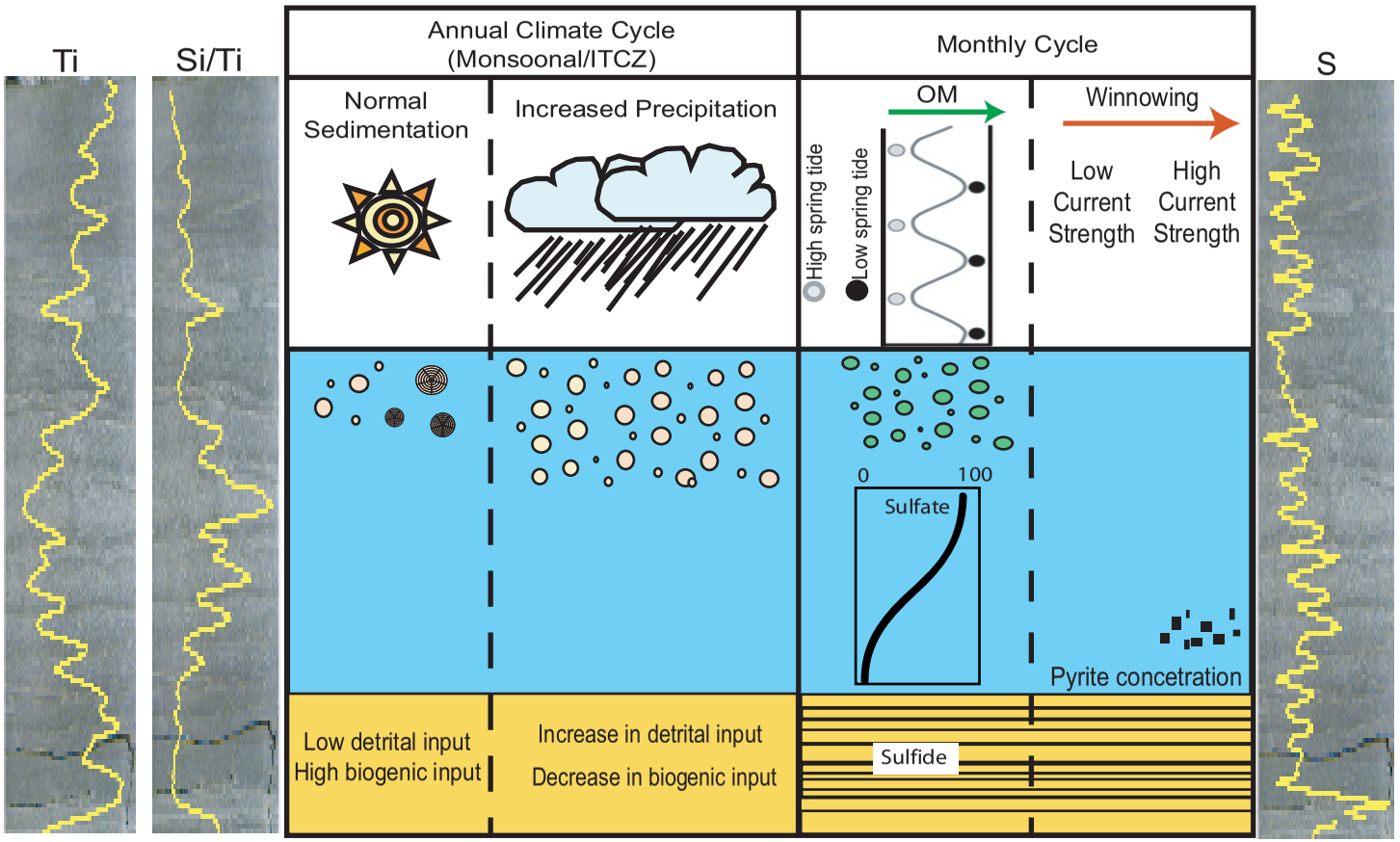


Figure 25. Depositional model for the distal Pride Shale sample, based on the XRF-scanner proxy data. An interpreted annual precipitation cycle is attributed to the summer monsoon or annual migration of the Intertropical Convergence Zone. Biogenic sedimentation dominates during times of low precipitation, while seasonal increases in precipitation are associated with enhanced input of terrigenous titanium. This results in an inverse relationship between Ti and Si.Ti. The redox proxy sulfur is interpreted as monthly, and can be due to either organic matter loading, where increased marine organic matter results in increased sulfide reduction, or an increase in current strength, resulting in winnowing of sediment, leaving a pyrite lag.

Figure 26. Outcrop view of the sampling site at Camp Creek, WV. Jacob's staff (1 m) for scale.

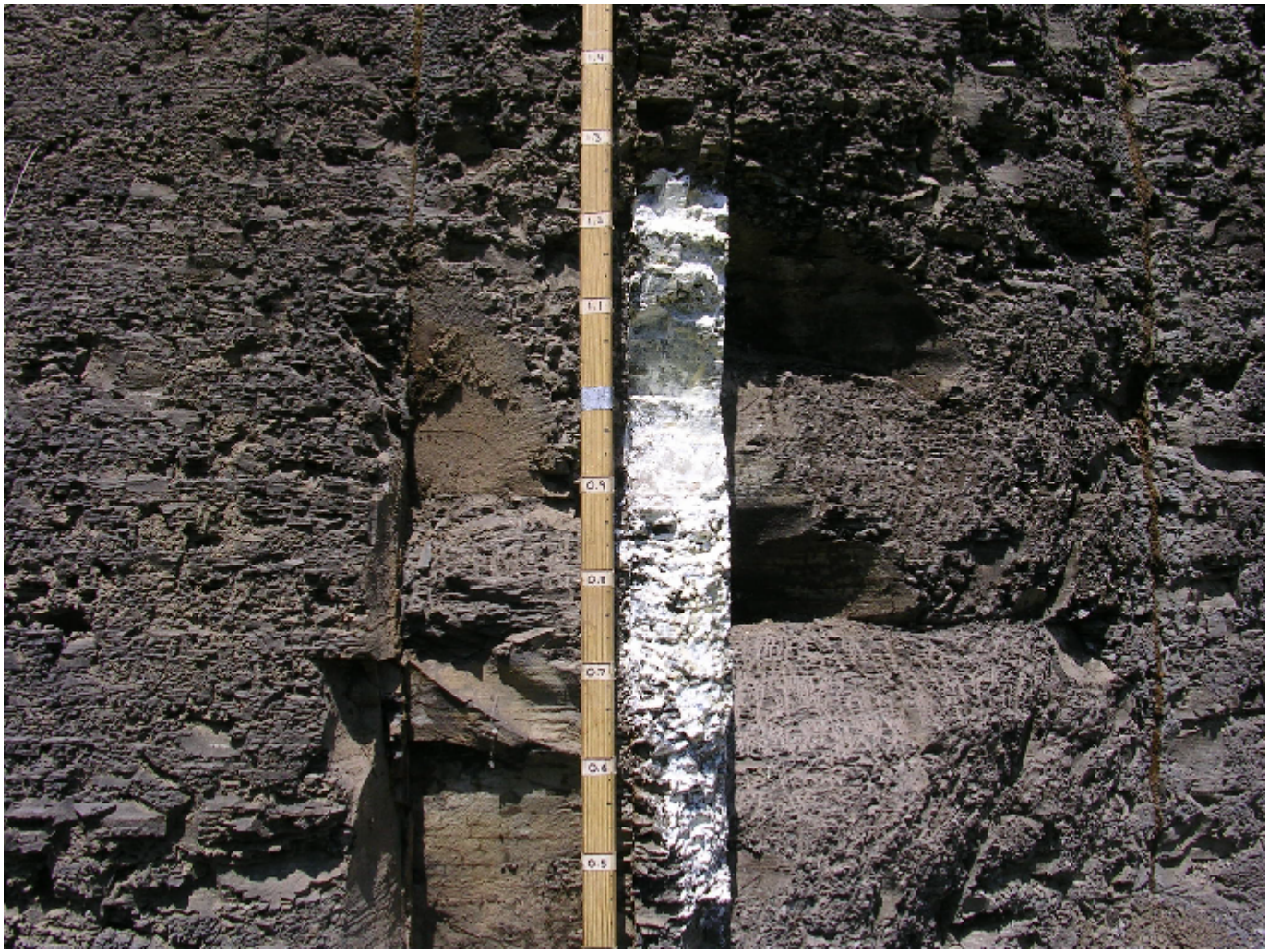

Figure 27. Photograph of the sampling method used to obtain an outcrop slab at Camp Creek in West Virginia. The outcrop was coated in layers of sodium silicate, rubber latex mold, and foam sealant, prior to extraction with a concrete saw.

to best resolve the cyclic tidal and seasonal cycles. Note that our discussion of the analysis of the proximal (I-77) sample is abbreviated, as the primary concepts have been developed above (section 3.2). This discussion will primarily focus on those aspects that differ from the distal analysis.

### 3.3.1 I-77 Sample Analysis

The I-77 outcrop (proximal prodeltaic setting) produced a slab that is 22 cm in length, with several gaps in the shale. This sample was analyzed on the Avaatech XRF-scanner using a 0.5 mm step size and both a 10 kV/1000 μA scan for 60 seconds and a 30 kV/1000 μA scan with a Pd-thin filter for 120 seconds.

Figure 28 displays a summary of the XRF-scanning results. The XRF data for titanium (Figure 28) shows an overall trend of darker layers containing increased titanium, while Si/Ti data increases in the lighter laminations (Figure 28). However, a crossplot of Si vs Ti and Ca vs Ti (Figure 31) shows a general positive correlation between Si and Ti, and a negative correlation between Ca and Ti. The positive correlation between Si and Ti differs markedly from the distal Pride Shale sample. We propose that this is due to the predominance of a detrital quartz source for the silicon in the proximal site, and a more biogenic silica source in the distal site.

Evolutive Harmonic Analysis of the titanium (Figure 29) and silicon/titanium data (Figure 30) from the proximal Pride Shale sample indicates more complicated, and less pervasive cyclic variability than observed in the distal Pride Shale sample. Table 2 summarizes the results for the proximal Pride Shale sample. The transient 23.8 mm signal

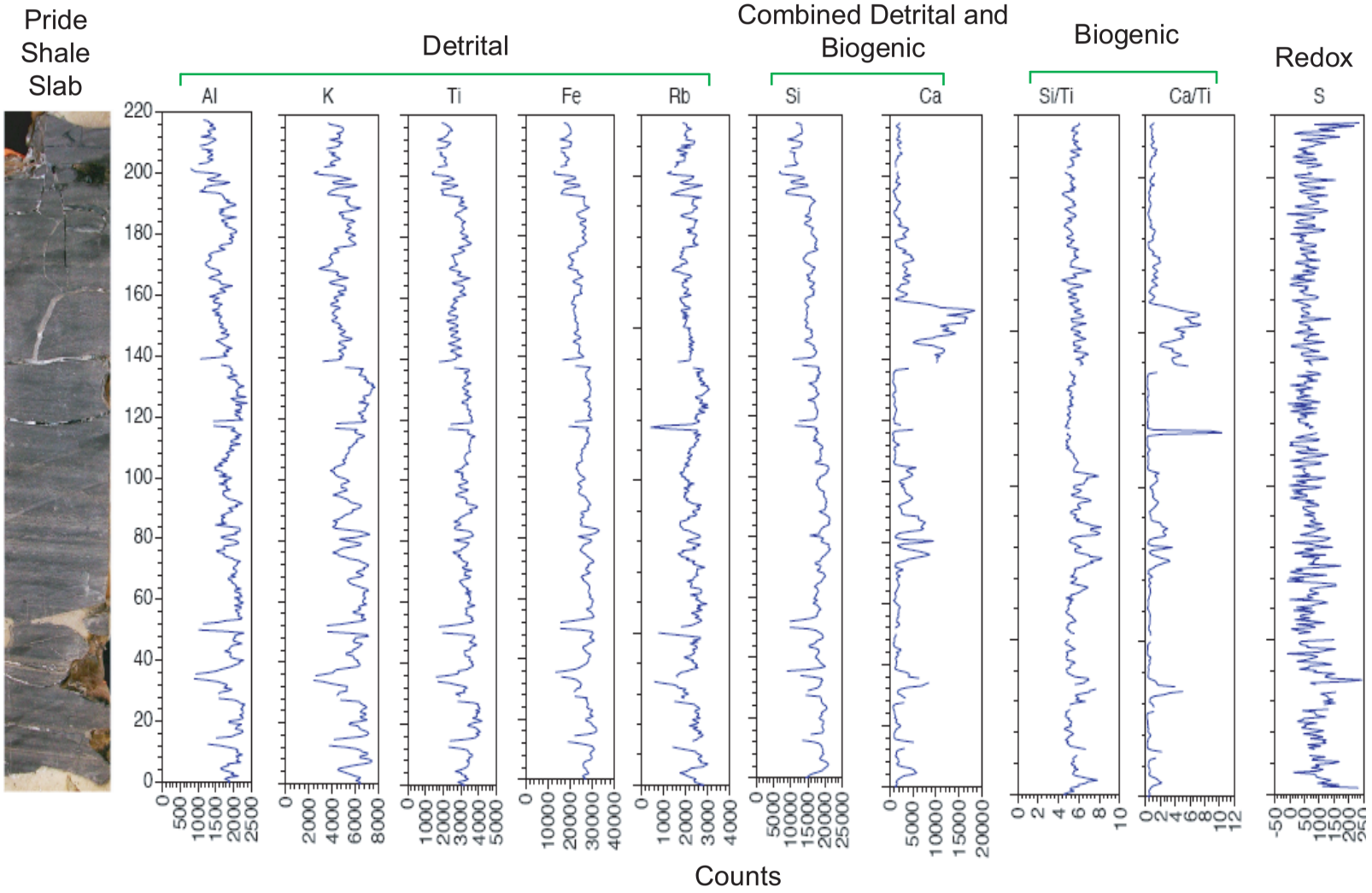


Figure 28. XRF-scanning results for the proximal Pride Shale sample, alongside a photograph of the analyzed interval. Select detrital, biogenic, and redox proxies are displayed. All results are expressed as XRF counts. Height axis is in millimeters.

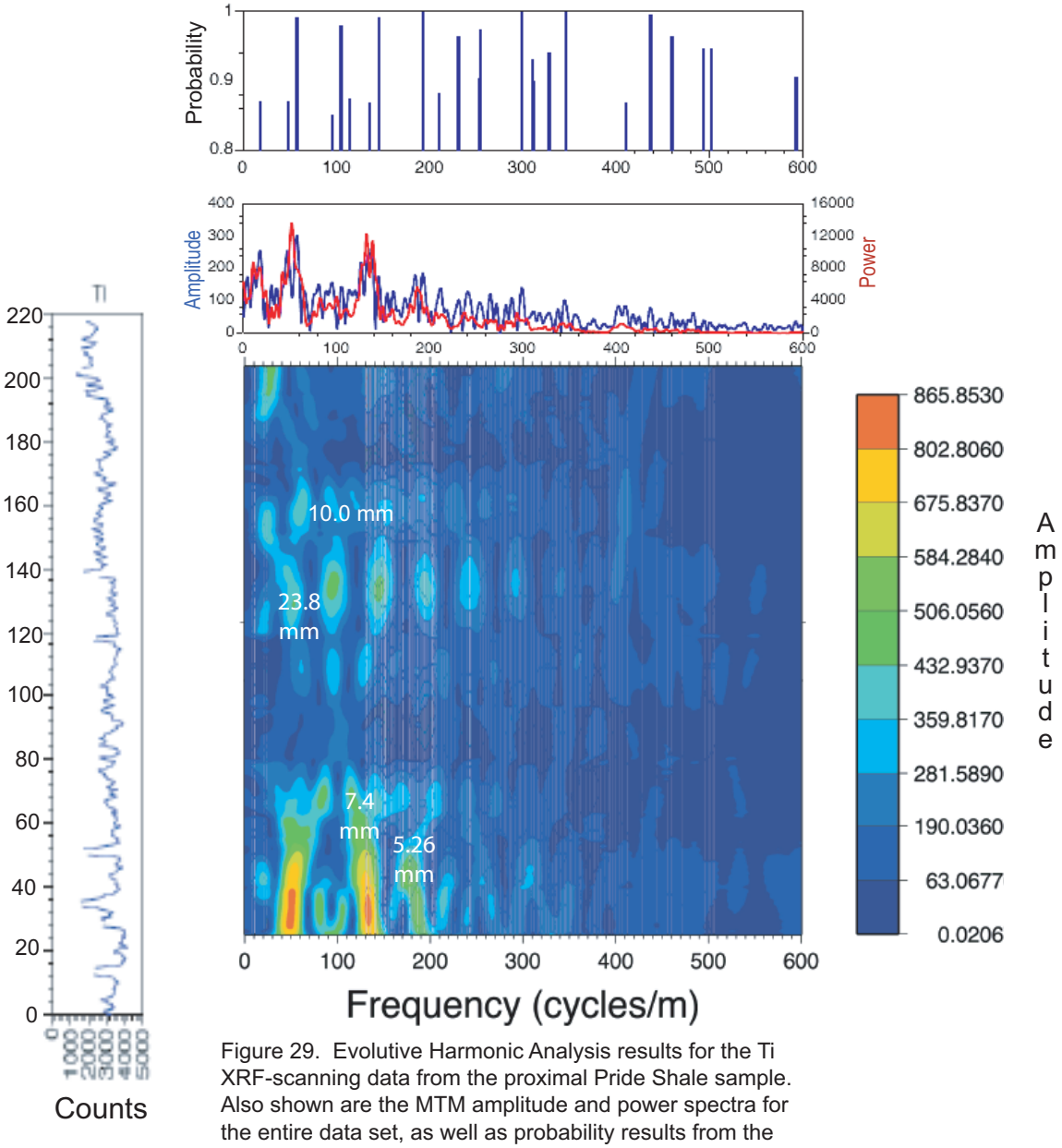


Figure 29. Evolutive Harmonic Analysis results for the Ti XRF-scanning data from the proximal Pride Shale sample. Also shown are the MTM amplitude and power spectra for the entire data set, as well as probability results from the MTM harmonic test.

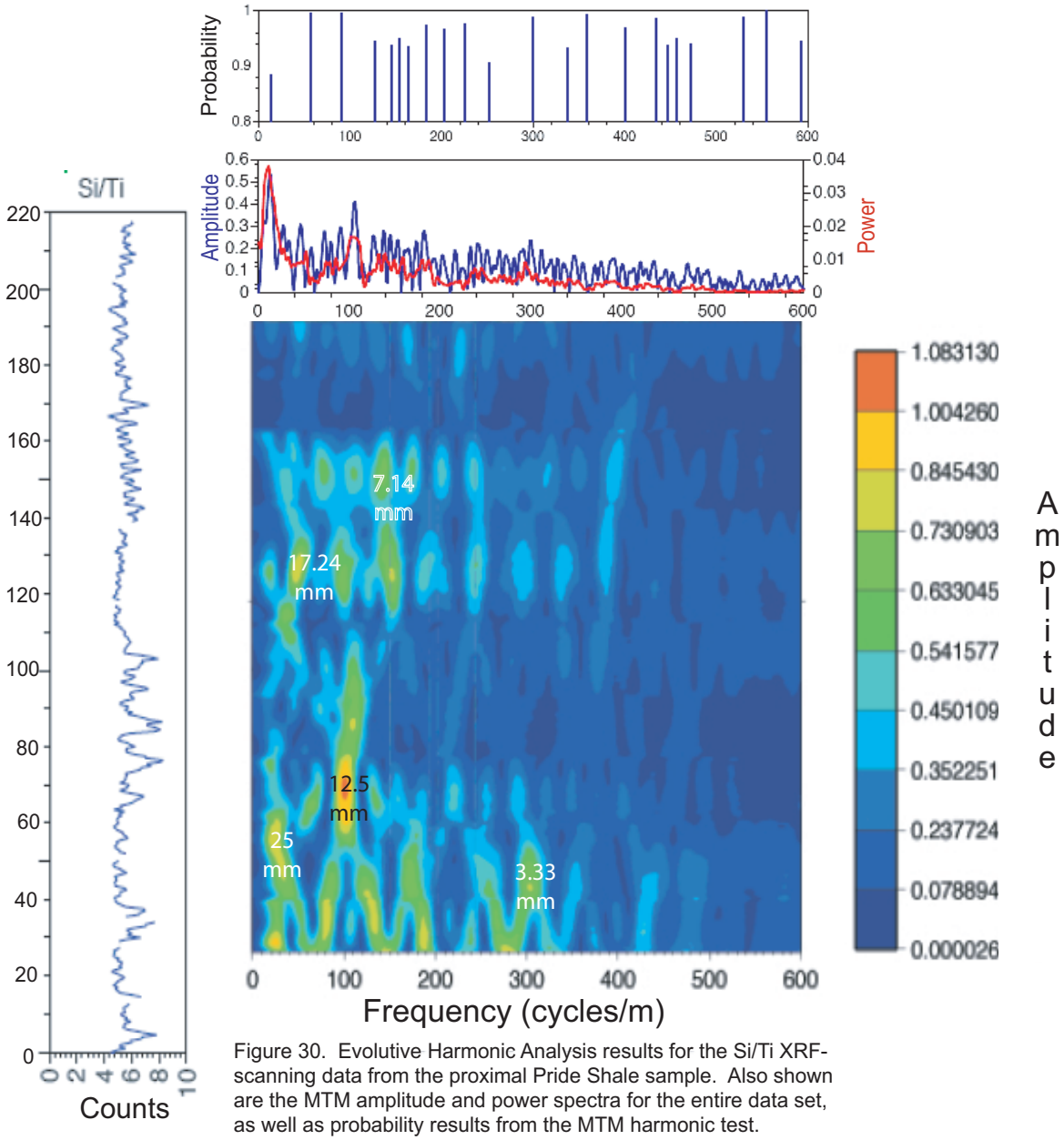


Figure 30. Evolutive Harmonic Analysis results for the Si/Ti XRF-scanning data from the proximal Pride Shale sample. Also shown are the MTM amplitude and power spectra for the entire data set, as well as probability results from the MTM harmonic test.

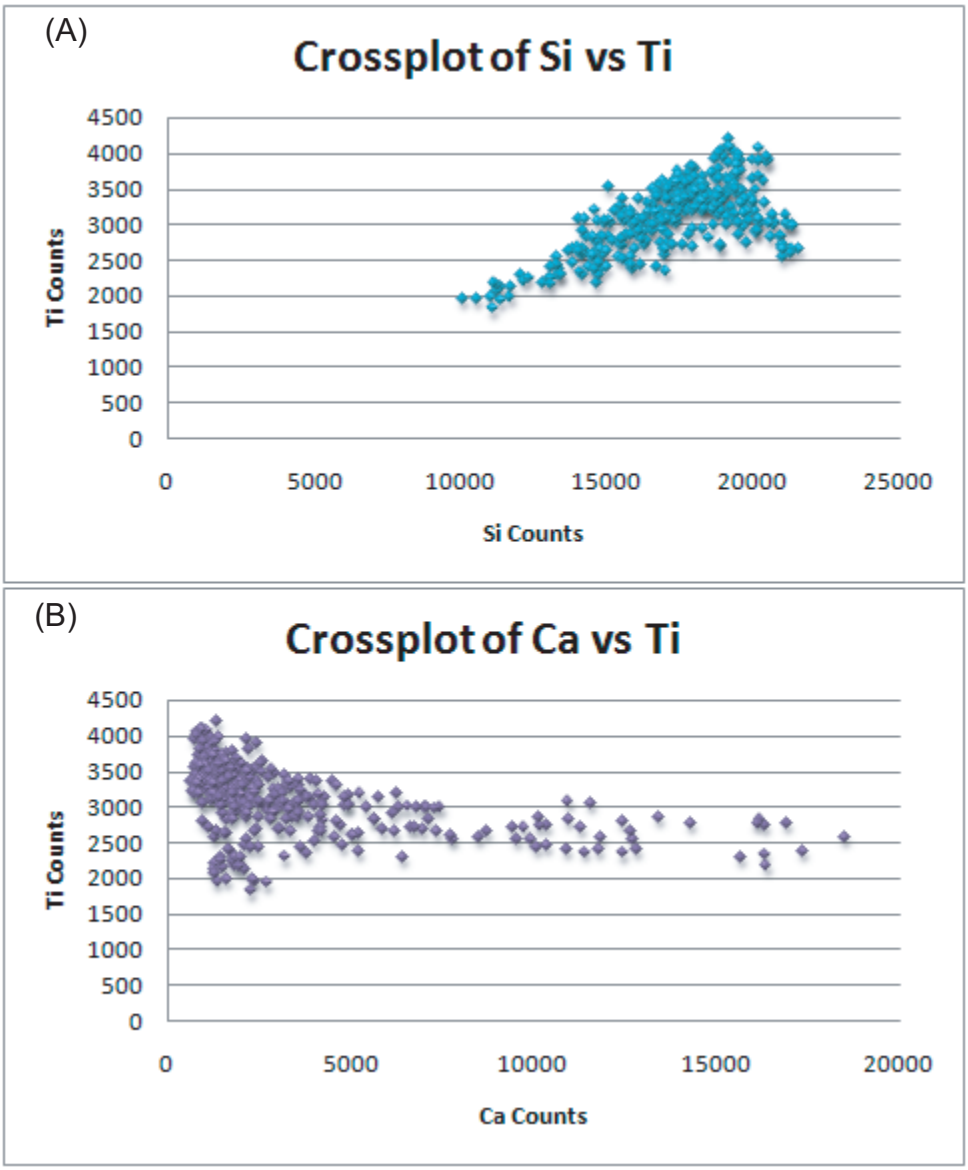


Figure 31. (A) Crossplot of the silicon and titanium XRF counts from the proximal Pride Shale sample. (B) Crossplot of the calcium and titanium XRF counts from the proximal Pride Shale sample. Figure 31B illustrates a similar overall inverse relationship as identified in the proximal sample, while Figure 31A shows a positive correlation. This may be due to different sources for the Si and Ca, with primarily a detritial silica origin for the silicon and primarily a biogenic origin for the calcium.

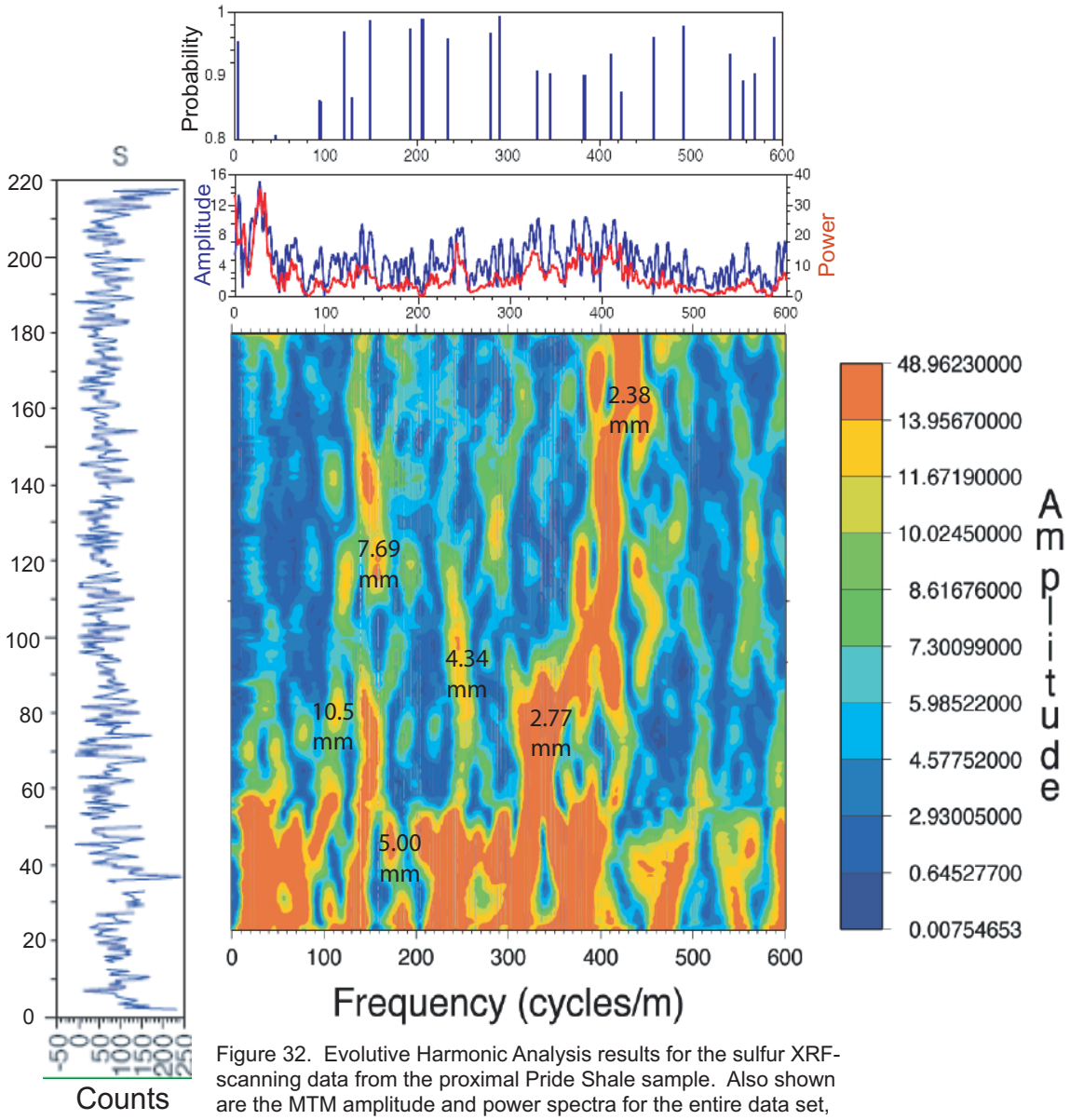


Figure 32. Evolutive Harmonic Analysis results for the sulfur XRF-scanning data from the proximal Pride Shale sample. Also shown are the MTM amplitude and power spectra for the entire data set, as well as probability results from the MTM harmonic test.

| Element | Spatial Period |
|---|---|
| Ti | 23.8 mm |
| | 10.0 mm |
| | 7.4 mm |
| | 5.26 mm |
| Si/Ti | 25 mm |
| | 17.24 mm |
| | 12.5 mm |
| | 7.14 mm |
| | 3.33 mm |
| S | 10.5 mm |
| | 7.69 mm |
| | 5.00 mm |
| | 4.34 mm |
| | 2.77 mm |
| | 2.38 mm |

Table 2. Observed spatial periods in the proximal Pride Shale sample.

observed in the Ti data, and the transient 25 mm cycle in the Si/Ti data, are similar to the ~27 mm signal found in the 16 cm slab from the distal sample.

The XRF data for sulfur shows no trend with light or dark laminations. Evolutive Harmonic Analysis of the sulfur data reveals a prominent cyclicity of 2.38 mm (Figure 32). The 2.38 mm signal is similar to the distal sample analysis, which exhibited a dominant 2.27 mm cycle. Thus, in contrast to the Ti and Si/Ti results, the sulfur data is characterized by a very high amplitude and persistent cycle in both the distal and proximal samples. More severe distortion of this signal in the proximal sample is likely the result of hiatus and enhanced bioturbation.

# CHAPTER 4

# CONCLUSIONS

## 4.1 Conclusions

In this study we have developed a new approach for the analysis of ancient tidal rhythmites. The methodology utilizes XRF-scanning to quantify multiple paleoenvironmental proxies at very high resolution, and these XRF proxy data are then evaluated using advanced spectra methods to discern tidal and seasonal cycles. As a case study, we have applied the approach to evaluate rhythmites of the Mississippian Pride Shale. Two specific hypotheses we have investigated are:

Hypothesis 1: The geochemistry of the Pride Shale rhythmites preserves multiple paleoenvironmental signals (e.g., detrital, biogenic, and authigenic contributions)

Hypothesis 2: The quality of the Pride Shale rhythmite record (completeness, etc.) varies from distal to proximal prodeltaic settings.

Relative to hypothesis 1, our results suggest that titanium, Si/Ti and sulfur data can serve as robust proxies for detrital, biogenic and authigenic contributions, respectively. However, the interpretation of Si/Ti requires some care, since it may also record changes in the contribution of quartz sand versus silt-sized sediment. In fact, our analysis suggests that

the Si/Ti record in the distal pro-delta primarily reflects changes in biogenic silica contribution. In contrast, we hypothesize that the Si/Ti record appears to reflect sand versus silt contribution in the proximal pro-delta.

Relative to hypothesis 2, spectral analysis of the XRF proxy data has resulted in the interpretation of a prominent annual cycle in the Ti and Si/Ti records, expressed at a period of ~27 mm (distal site). This forcing may be linked to annual movement of the Intertropical Convergence Zone, or to the annual summer monsoon. The interpreted annual cycle is less persistent and robust in the proximal sample of the Pride Shale, indicating a poorer quality record closer to the shoreline. This is likely due to more frequent disturbance of the sediments by bottom currents and/or bioturbation. Thus, we can conclude that distal pro-delta locations should preserve a more pristine record of the seasonal and tidal rhythms. Such locations should be targeted for future work.

Spectral analysis of the sulfur data suggests a prominent monthly signal, expressed at a period of ~2.27 mm (distal site). The source of this forcing may be associated with enhanced marine organic matter concentration and sulfate reduction during exceptionally high monthly spring tides. Alternatively, sulfur enrichment may be attributable to winnowing of fine-grained sediment during exceptionally low monthly neap tides. In the latter case, the sulfur record constitutes a lag of disseminated pyrite.

In future studies, a better sample of the Pride Shale is needed in order to discern between an annual ITCZ and summer monsoon forcing. The ideal sample would contain a daily signal, so that one could count the number of days in a year during the Mississippian, as well as still contain the annual climatic cycle. Once laminae associated with individual days are identified, we can potentially count the number of days elapsed, to determine whether the

increase in detrital input occurs during the peak of the summer monsoon, or alternatively, when the ITCZ is overhead.

Furthermore, a very long core of the Pride Shale, or multiple smaller samples throughout the unit, may also reveal an orbital forcing that controls the intensity of the monsoonal/ITCZ cycle (e.g., Ruddiman, 2001). The amount of solar insolation reaching the low latitudes (where the Pride Shale basin was located) varies with an orbital precession rhythm of ~20 kyr (Ruddiman, 2001). Therefore, a stronger relative monsoonal/ITCZ signal (eg. titanium flux) would occur during higher summer insolation, associated with changes in the earth's precession. Future work will allow us to better constrain the tidal rhythms, and yield important insight into paleoclimate change during the last ice house.

# Appendix 1

## Locality Description

### 0.5 mm Data

A boulder was collected in the field from an Old Spanishburg Road outcropping of the Pride Shale, located off of Route 19 in Spanishburg, WV (see topographic map). To get to sampling area, take I-77 North to exit 20 at Camp Creek, West Virginia. Turn right onto Route 19 south. Approximately 8.5 miles on Route 19 South, cliffs of the Pride Shale outcrop on the right side of the road. Boulder sample was taken from this area.

### I-77 Data

An outcrop slab from Interstate 77 at exit 20, Camp Creek, WV was obtained using a concrete saw and various adhesives. This outcropping contains a long record of the Pride Shale, and begins to grade into the Glady Fork Member near the top of the section. Permission for sampling along an interstate was obtained via the West Virginia Highway Patrol Authority. To access outcrop, take Interstate 77 to exit 20 at Camp Creek, West Virginia (see topographic map). Pull alongside of Interstate 77 approximately 0.5 miles past exit 20. Outcropping sample was cut from the lower portion of the Pride Shale.

Topographic maps from the West Virginia Geological Survey
http://www.wvgs.wvnet.edu/www/maps/maps.htm

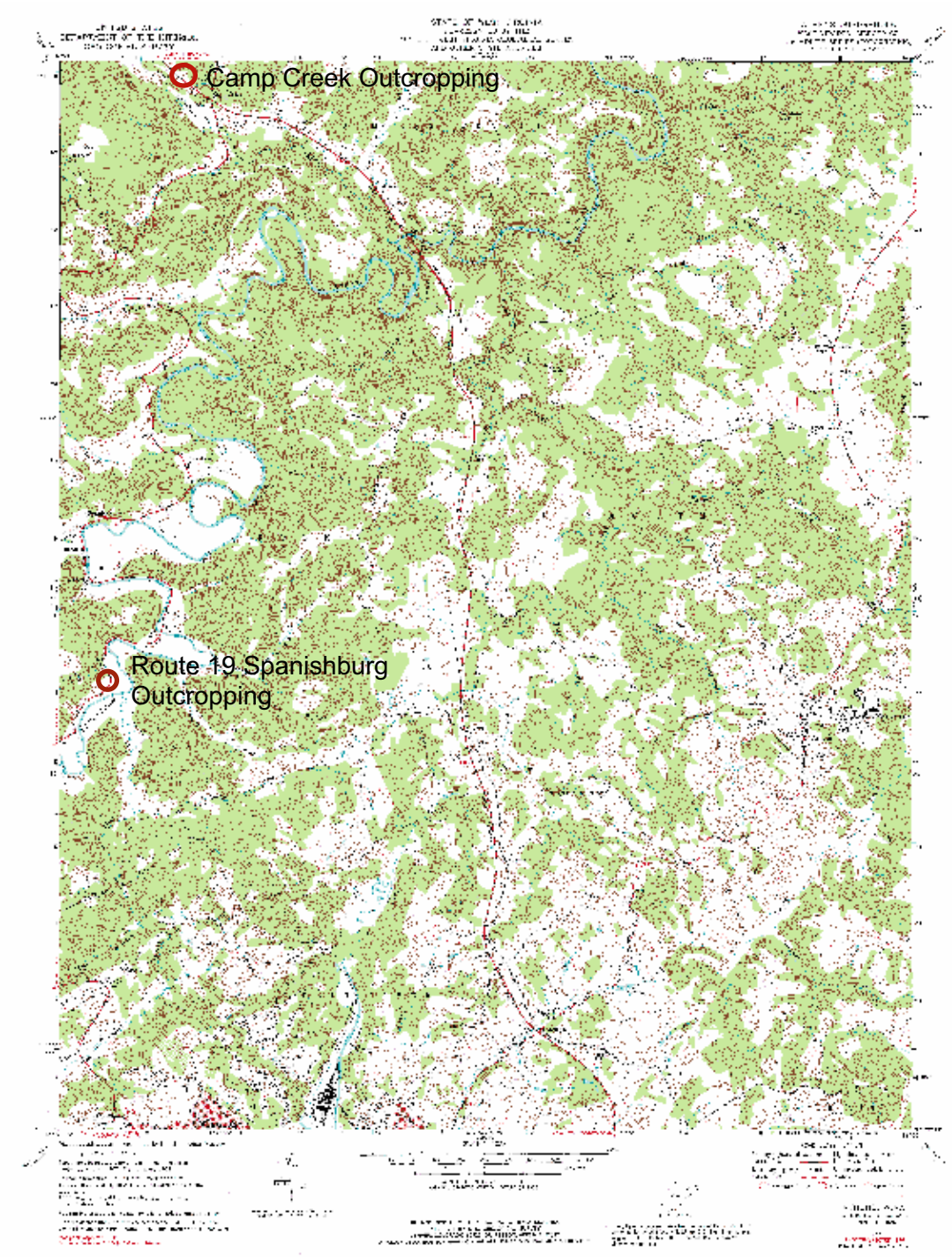


Topographic Map illustrating the location of the sample taken in situ from the Pride Shale using a concrete saw and combination of adhesives at the Camp Creek exit outcropping. The map also illustrates the location of the boulder sample taken along Route 19 in Spanishburg, WV. Topographic maps from the West Virginia Geological Survey at http://www.wvgs.wvnet.edu/www/maps/maps.htm

References

Archer, A.W., Kvale, E.P., Johnson, H.R., 1991, Analysis of modern equatorial tidal periodicities as a test of information encoded in ancient tidal rhythmites, in Smith, D.G., Reinson, G.E., Zaitlin, B.A., Rahmani, R.A. (eds.), Clastic Tidal Sedimentology, Memoir, vol. 16. Canadian Society of Petroleum Geologists, p. 189– 196.

Archer, A. W. (1994). "Extraction of sedimentological information via computer-based image analyses of gray shales in Carboniferous coal-bearing sections of Indiana and Kansas, USA." Mathematical Geology 26: 47-65.

Archer, A.W., Kuecher, G.J., and Kvale, EP (1995). "The role of tidal-velocity asymmetries in the deposition of silty tidal rhythmites (Carboniferous, Eastern Interior Coal Basin, USA)." Journal of Sedimentary Research Section A - Sedimentary Petrology and Processes 65(2): 408-416.

Archer, A. W. (1995). "Modeling of Cyclic Tidal Rhythmites based on a Range of Dirunal to Semidiurnal Tidal-station Data." Marine Geology 123: 1-10.

Berger et al., (1989). “Influence of the changing lunar orbit on the astronomical frequencies of pre-Quaternary insolation parameters.” Paleoceanography 4:555-564.

Berner, Robert A. (1984). “Sedimentary pyrite formation: An update*.” Geochimica et Cosmochimica Acta 48: 605-615.

Berner, Robert A. (1970) “Sedimentary pyrite formation.” American Journal of Science 268: 1-23

Bertrand, P., Shimmield, G.B., Martinez, P., Grousset, F.R., Jorissen, F., Paterne, M., Pujol, C., Bouloubassi, I., Buat-Menard, P., Peypouquet, J.P., Beaufort, L., Sicre, M.A., Lallier-Verges, E., Foster, J.M., and Ternois, Y. (1996). “The glacial ocean productivity hypothesis: the importance of regional temporal and spatial studies.” Marine Geology 130 (1,2): 1-9

Boggs, S. (1987) Principles of Sedimentology and Stratigraphy, Columbus, Ohio, Merrill Publishing Co., 784 p.

Cecil, C. B., and Englund, K.J. (1989). “Origin of coal deposits and associated rocks in the Carboniferous of the Appalachian Basin.” Coal and hydrocarbon resources of North America. C. B. Cecil, Eble, C.F. Washington D.C., Am. Geophysical Union. 2: 84-104.

Cooper, B.N., 1961, Grand Appalachian Field Excursion, Field Trip 1 of Geological Society of America Annual Meeting, Cincinnati, Ohio: Virginia Polytechnic Institute, Engineering Extension Series, Geological Guidebook 1, 187 p.

Davis, C., Pratt, L.M., Sliter, W.V., Mompart, L., and Murat, B. (1999). Factors Influencing Organic Carbon and Trace Metal Accumulation in the Upper Cretaceous La Luna Formation of the western Maracaibo Basin, Venezuela. Evolution of the Cretaceous Ocean-Climate System. E Barrera and C. Johnson, Geological Society of America, Boulder: 203-230.

Devol, A. H.,, and Ahmed, S.I. (1981). "Are high rates of sulphate reduction associated with anaerobic oxidation of methane?" Nature 291: 407-408.

DiVenere, V. J., and Opdyke, N.D. (1991). "Magnetic polarity stratigraphy in the uppermost Mississippian Mauch Chunk Formation, Pottsville, Pennsylvania." Geology 19: 127-130.

Ekdale, A.A., Muller, L.N., Novak, M.T. (1984). “Quantitative ichnology of modern pelagic deposits in the abyssal Atlantic” Palaeogeography, Palaeoclimatology, Palaeoecology 45:189-223.

Englund, K.J. (1989), “Camp Creek interchange section”, in Cecil, C.B., and Eble, C., eds., Carboniferous Geology of the Eastern United States: 28th International Geological Congress, Field Trip Guidebook T143: 91-93.

Englund, K. J., and Thomas, R.E. (1990). "Late Paleozoic Depositional Trends in the Central Appalachian Basin." U. S. Geological Survey Bulletin 1839-F: 19.

Ettensohn, F.R., 1994, Tectonic control on formation and cyclicity of major Appalachian unconformities and associated stratigraphic sequences: *in* Dennison, J.M. and Ettensohn, F.R., eds., Tectonic and Eustatic Controls on Sedimentary Cycles, SEPM Concepts in Sedimentology and Paleontology, v. 4, p. 217-242.

Frouin, M., Sebag, D., Laignel, B., Ogier, S., Verrecchia, E.P., Durand, A. (2006). "Tidal rhythmites of the Marais Vernier Seine Estuary, France and their implications for relative sea-level." Marine Geology 235: 165-175.

Golonka, J., Ross, M.I., and Scotese, C.R. (1994). "Phanerozoic paleogeographic and paleoclimatic modeling maps: Pangea: Global environments and resources." Canadian Society of Petroleum Geologists Memoir 17: 1-47.

Haug, G. H., Gunther, D.; Peterson, L.C., Sigman, D.M., Hughen, K.A., Aeschlimann, B. (2003). "Climate and the Collapse of the Maya Civilization." Science 299: 1731-1735.

Haug, G.H., Hughen, K.A., Sigman, D.M., Peterson, L.R., and Rohl, U. (2001). "Southward Migration of the Intertropical Convergence Zone Through the Holocene.” Science, 293:1304-1307.

Hovikoski, J., Rasanen, M., Gingras, M., Ranzi, A., and Melo, J. (2008) “Tidal and seasonal controls in the formation of Late Miocene inclined heterolithic stratification deposits, western Amazonian foreland basin.” Sedimentology, 55: 499-530.

Hovikoski, J., Rasanen, M., Gingras, M., Roddaz, M., Brusset, S., Hermoza, W., Pittman, L., and Lertola, K. (2005). “Miocene semidiurnal tidal rhythmites in Madre de Dios, Peru.” Geology, 33: 177-180.

Jaeger, J. M., and Nittrouer, C.A. (1995). "Tidal controls on the formation of fine-scale sedimentary strata near the Amazon river mouth." Marine Geology 125: 259-281.

Jenkins, R. (1999). X-Ray Flourescence Spectrometry, 2nd Edition: New York, John Wiley and Sons, 207 pp.

Kvale, E. P. (2003). Tides and Tidal Rhythmites. Encyclopedia of Sediments and Sedimentary Rocks. G. Middleton, Kluwer Academic: 741-744.

Kvale, E. P. (2006). "The Origin of Neap-Spring Tidal Cycles." Marine Geology 235: 5-18.

Lantzy, R. and Mackenzie, F. (1979). Atmospheric Trace Metals: Global Cycles and Assesment of Man’s Impact. Geochimica Cosmochimica Acta 43, 522-536.

Libes, S. (2005). An Introduction to Marine Biogeochemistry. Ann Arbor, Copley Custom Textbooks.

Lyons, T, Werne, J, Hollander, D, and Murray, R. (2003). “Contrasting Sulfur Geochemistry and Fe/Al and Mo/Al Ratios Across the Last Oxic-to-Anoxic transition in the Cariaco Basin, Venezuela.” Chemical Geology 195: 131-157.

Mazumder, R. (2004). “Implications of lunar orbital periodicity from the Chaibasa tidal rhythmite (India) of late Paleoproterozoic age.” Geology 32 (10): 841-844.

Mazumder, R., and Arima, M. (2004). "Tidal Rhythmites and their Implications." Earth-Science Reviews 69: 79-95.

Meyers, S. R., Sagemon, B.B; and Hinnov, L.A (2001). "Integrated Quantitative Stratrigraphy of the Cenomanian-Turonian Bridge Creek Limestone Member using Evolutive Harmonic Analysis and Stratigraphic Modeling." Journal of Sedimentary Research 71(4): 628-644.

Miller, D.J. (1998). Depositional Environments and Sequence Stratigraphy of Upper Mississippian Strata in the Central Appalachian Basin. Geological Sciences. Blacksburg, Virginia Polytechnic Institute and State University. Doctor of Philosophy: 87.

Miller, D.J. and Eriksson., K.A. (2000). "Sequence stratigraphy of Upper Mississippian strata in the central Appalachians: A record of glacioeustasy and tectonoeustasy in a foreland basin setting." AAPG Bulletin - American Association of Petroleum Geologists 84(2): 210-233.

Miller, D.J. and Eriksson., K.A. (1997). "Late Mississippian prodeltaic rhythmites in the Appalachian basin: a hierarchical record of tidal and climatic periodicities." Journal of Sedimentary Research 67(4): 653-660.

Miller, M.S. (1974). "Stratigraphy and coal beds of Upper Mississippian and Lower Pennsylvanian rocks in southwestern Virginia." Virginia Division of Mineral Resources Bulletin 84: 211.

Neal, D.W. (1994). "Late Mississippian anoxia in the central Appalachian foreland basin" (abstract). Geological Society of America, Abstracts with Programs 26 (7): A-247.

Niewohner, C., Hensen, C., Kasten, S., Zabel, M., Schulz, H.D. (1997). "Deep Sulfate Reduction Completely Mediated by Anaerobic Methane Oxidation in Sediments of the Upwelling Area off Namibia." Geochimica et Cosmochimica Acta 62(3): 455-464.

Rasband, Wayne. ImageJ 1.40g (computer software), National Institutes of Health.

Reading, H. and Collinson, J., 1996, Clastic Coasts in Reading, H. (ed.) Sedimentary environments, processes, facies, and stratigraphy v. 3, Blackwell Science. 154-231.

Reger, D.B. (1926). Mercer, Monroe, and Summers Counties: West Virginia Geological Survey County Report, 963 p.

Rice, C.L., and Schwietering, J.F. (1988) “Fluvial deposition in the Central Appalachians during the early Pennsylvanian.” U.S. Geological Survey Bulletin, Report B: B1-B10.

Richter, T.O., van der Gaast, S., Koster, B., Vaars, A., Gieles, R., de Stigter, H.C., de Haas, H., van Weering, T., 2006, The Avaatech XRF core scanner; technical description and applications to NE Atlantic sediments, in Rothwell, R.G. (ed.), New techniques in sediment core analysis, Geological Society of London, p. 39-50.

Ruddiman, W. F. (2001). Earth's Climate Past and Future. New York, W.H. Freeman & Co. pp. 33-35.

Sageman, B.B., and Lyons, T.W., 2004, Geochemistry of fine-grained sediments and

sedimentary rocks, in Mackenzie, F.T. (ed.), Sediments, Diagenesis, and Sedimentary Rocks: Treatise on Geochemistry v. 7, Elsevier, p. 115-158.

Scotese, C. (1986). Atlas of Paleozoic basemaps. Atlas of Paleozoic basemaps, paleoceanographic mapping project, University of Texas, Institute for Geophysics.

Sonett, C. P., Kvale, E.P., Zakharian, A., Chan, M.A., Demko, T.M. (1996). "Late Proterozoic and Paleozoic Tides, Retreat of the Moon, and Rotation of the Earth." Science 273(5271): 100-104.

Thomson, D.J. (1982). "Spectrum estimation and harmonic analysis" IEEE Proceedings 70: 1055–1096.

Waliser, D. E., and Gautier, C. (1993). "A satellite derived climatology of the ITCZ" Journal of Climate 6: 2162-2174.

Wells, M. R., Allison, P.A., Piggott, M.D., Gorman, G.J., Hampson, G.J., Pain, C.C., Fang, F. (2007). "Numerical Modeling of Tides in the late Pennsylvanian Midcontinent Seaway of North America with Implications for Hydrography and Sedimentation." Journal of Sedimentary Research 77: 843-865.

Williams, G. E. (1991). "Tidal rhythmites; key to the history of the Earth's rotation and the lunar orbit." Journal of Physics of the Earth 38(6): 475-491.

Williams, G.E. (1997) "Precambrian length of day and the validity of tidal rhythmite paleotidal values." Geophysical Research Letters 24(4): 421-424.

Yarincik, K. M., Murray, R.W. (2000b). "Climatically Sensitive Eolian and Hemipelagic Deposition in the Cariaco Basin, Venezuela, Over the Past 578,000 Years: Results From Al/Ti and K/Al " Paleoceanography 15(2): 210-228.